Intra- and inter-field compositional changes of oils from the Misoa B4 reservoir in the Ceuta Southeast Area (Lake Maracaibo, Venezuela)

G. Márquez [a,⇑], M. Escobar [b,c], E. Lorenzo [a], L. Duno [d], N. Esquinas [e], J.R. Gallego [e]

[a] Departamento de Ingeniería Minera, Mecánica y Energética, Universidad de Huelva, 21819 Huelva, Spain
[b] CARBOZULIA, Avenida 2 No. 55-185, Casa Mene Grande, Maracaibo 4002 A, Venezuela
[c] Postgrado de Geología Petrolera, Facultad de Ingeniería, Universidad del Zulia, Maracaibo 10482, Venezuela
[d] PDVSA, Calle 77, Edificio PDVSA 5 de Julio, Maracaibo 4002, Venezuela
[e] Departamento de Explotación y Prospección de Minas, Universidad de Oviedo, C/G. Gutiérrez, 33600 Mieres, Spain

Abstract

Here we analyzed oil samples from 35 wells in the Ceuta Southeast Area (Lake Maracaibo Basin, north- western Venezuela) in order to evaluate lateral intra-reservoir continuity in the Misoa B4 unit. Biomarkers, isotopic signature, and also V and Ni were examined using gas chromatography–mass spectrometry (GC–MS), isotope ratio mass spectrometry (IRMS), and inductively-coupled plasma atomic emission spectroscopy (ICP-AES). Multivariate statistical analysis was also applied to obtain useful information from geochemical data. On the basis of the characterization of these samples, we conclude that they all fall into various oil families derived from two pulses of hydrocarbon generation, migration and accumulation from the calcareous La Luna source rock, deposited in an anoxic marine environment under reducing conditions. Thus, these oils are a mixture of an earlier biodegraded, less mature oil charge and a later fresh non-biodegraded oil recharge. In addition, we applied asphaltene pyrolysis to one (LG-62) of the three ‘‘anomalous” oils. The LG-62 sample was confirmed as an almost ‘‘pure” paleobiodegraded end-member, whereas the VLF-3020 oil was tentatively classified as the unaltered end-member oil-type. Finally, the GC fingerprints and Fourier Transform Infra Red (FTIR) spectroscopic indices of the oils were used to detect minor variations in composition that are indicative of reservoir compartmentalization.

Keywords:
Ceuta Southeast Area Misoa B4 sands, Reservoir compartmentalization Generation pulses, FTIR indices

1. Introduction

The Lake Maracaibo Basin lies in northwestern Venezuela and covers approximately 50,000 km2. The principal petroleum source rock is the Cretaceous La Luna Formation, although others also generated hydrocarbons [70,71,75]. The main petroleum accumulations are found in the Eocene and Miocene deltaic sandstones [72]. In turn, the region known as ‘‘Ceuta” is located near the Ceuta locality on the southeastern side of the Lake, 90 km southeast of the city of Maracaibo (Zulia State; see Fig. 1). The ‘‘Ceuta” region has been divided into various areas; one of the most important of these is ‘‘Area 8”, also known as ‘‘Ceuta Southeast”. This area covers approximately 70 km2 and includes the following oilfields: onshore Tomoporo and Franquera and offshore Tomoporo (also named Lagotreco).

Previous organic geochemical studies ([71,46]; among others) of the oils from the study area did not reveal great differences with respect to their origin and maturation, thereby suggesting that they originated from a mature marine source rock (the carbonate La Luna Formation). It has also been reported (e.g. [25,47]) that Eocene crude oils produced in the southeastern part of Lake carbons and relatively high concentrations of resin compounds and asphaltenes. This composition could be explained by the fact that the medium to heavy crude oils produced in the aforementioned region are a mixture of an earlier charge of Eocene oil, which had been altered by biodegradation, and a later fresh unaltered oil charge originated from the same source rock (La Luna) during post-Oligocene times [69,72].

Here we examined a set of 35 samples from oil wells in the Eocene B4 reservoir (~150 °C) (nearly 5000 m depth) of the Tomoporo (8), Lagotreco (19), and Franquera (8) fields. We addressed the origin, biodegradation, and thermal maturity of these samples and identified contributions of end-member oil types. Furthermore, we sought to determine intra- and inter-field compositional changes in samples and thus to evaluate lateral intra-reservoir continuity and, when possible, to delineate compartments in the study area. This information can be of great use for future EOR processes and petroleum geochemistry research in Ceuta and other eastern sectors of the Lake Maracaibo Basin.

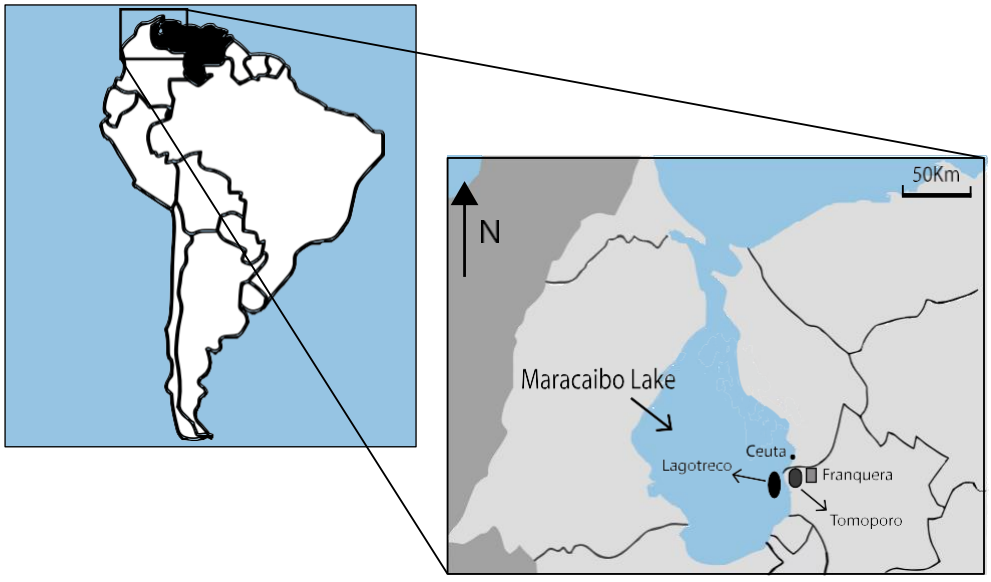

Fig. 1. Sketch map of the Lake Maracaibo region showing the relative position of the Lagotreco, Tomoporo, and Franquera oilfields.

2. Geological setting

The geology of northern Venezuela is conditioned by the interaction of the Caribbean, North American and South American plates [40]. In this general context, various authors ([39,50,43,15,20,44]; among others) have classified the sedimentary column in the eastern part of the Maracaibo Basin into several tectono-stratigraphic units: (i) a Lower to Upper Cretaceous

passive margin succession; (ii) a transition to a compressive regime in the Late Cretaceous–Early Paleocene, when collision and obduction of the Pacific volcanic arc overrode the South American plate and emplaced the Lara nappes; (iii) a Late Paleocene–Middle Eocene foreland basin succession in front of the volcanic arc; and (iv) a Late Eocene–Pleistocene sequence related to the collision of the Panama arc with the South American plate.

The southeastern margin of the Lake Maracaibo is bounded to the north by the Tomoporo fault, to the west by the Pueblo Viejo fault, to the east by the Moporo-1X structure and, finally, to the south by the R-5 secondary fault (see Fig. 2; [61]). The XE ‘‘Fallas Principales” Pueblo Viejo fault belongs to a group of normal faults originated in the Jurassic rifting [63]. However, as it was reactivated as a result of the emplacement of the Lara nappes [14], it is currently a N–S trending sinistral transform fault that dips steeply (70°) to the east. The Tomoporo R-1 and R-3 secondary structures (see Fig. 2) are E–W trending, 55–65° north-dipping echelon normal faults transversal to the main faults. Both structures were originated by extension during the appearance of the NW–SE outlying height located in the center of the current Lake Maracaibo Basin, within the period of active continental drift [2]. The Andean uplift explains the inversion of these latter secondary faults and the emergence of the antithetic structures associated with them [7]. As a final point, the Corredor 1, 2 and 3 faults, as well as the Moporo-1X faulting (see Fig. 2), are NW–SE trending and east-dipping transcurrent sinistral faults, generated as a result of the emplacement of the Lara nappes. Later on, compressive tectonic stresses in the region currently occupied by the Lake Maracaibo Basin reactivated and reversed these faults, thereby generating a flower structure [17]. It is feasible that the faults described led to distinct B4 reservoir compartments in our study area, thus suggesting a subdivision into six blocks (see Fig. 2). Basically, Blocks I, II, III and VI are gently dipping homoclinal blocks, differentiated by dip angles and dip directions of rock strata. In particular, the strata of Blocks I and III show a NE–SW orientation and a 5–7° dip towards the S–SE [23]. Regarding Block II, the homoclinal structure also shows a NE–SW orientation, but this block dips to the northwest [34], whereas Block VI (Franquera) is a W–E trending and steeply (3°) south-dipping homocline. Finally, two blocks (IV and V) are conformed by an anticlinal structure: Block IV with an anticlinal axis that has a SW–NE orientation and flanks dipping moderately (5–10°) to the NW, SW and SE, and Block V with a N–S axis trend and gently (3–5°) dipping flanks [14].

The stratigraphic column of Area 8 essentially consists of sedimentary rocks from Cretaceous and Cenozoic ages (Fig. 3) and displays the following lithological characteristics, from bottom to top: Río Negro (coarse-grained, arkosic, and fine-grained sandstones); Apón (grey limestones and shales); Lisure (sandstones alternating with glauconitic limestones and shales); Maraca (biomicritic limestones); La Luna (organic matter-rich, black limestones and calcareous clays); Colón Formation (grey shales); Mito Juan (siltstones); Guasare (limestones and sandstones); Misoa (fluviodeltaic sandstones, limonites, lutites, and some limestone) beds); Paují (grey shales); La Rosa (shales alternating with sandstones); Lagunillas (sandstones and carbonaceous shales); La Puerta (claystones, sandstones, coal, and conglomerates); Onia (sandstones, claystones and siltstones) and the El Milagro Formation—coarse-grained sandstones and conglomerates ([82,37,48]; and references herein). The Cogollo Group comprises the Apón, Lisure and Maraca formations (see Fig. 3). Detailed information on the Cretaceous and Tertiary stratigraphy of the

study area was provided by Boesi et al. [10].

The producing horizon under study is the Eocene Misoa Formation, which can be divided into several units termed, from top to bottom, Sands ‘‘A”, ‘‘B”, and ‘‘C” [79]. The Misoa sandstones in all the units are massive and show good vertical permeability within each unit [81]. Subsequently, ‘‘B” Sands can be divided in nine minor intervals (B1 to B9). These horizons indicate a transition from a deltaic environment (B6 to B9) to a restricted coastal environment [76].

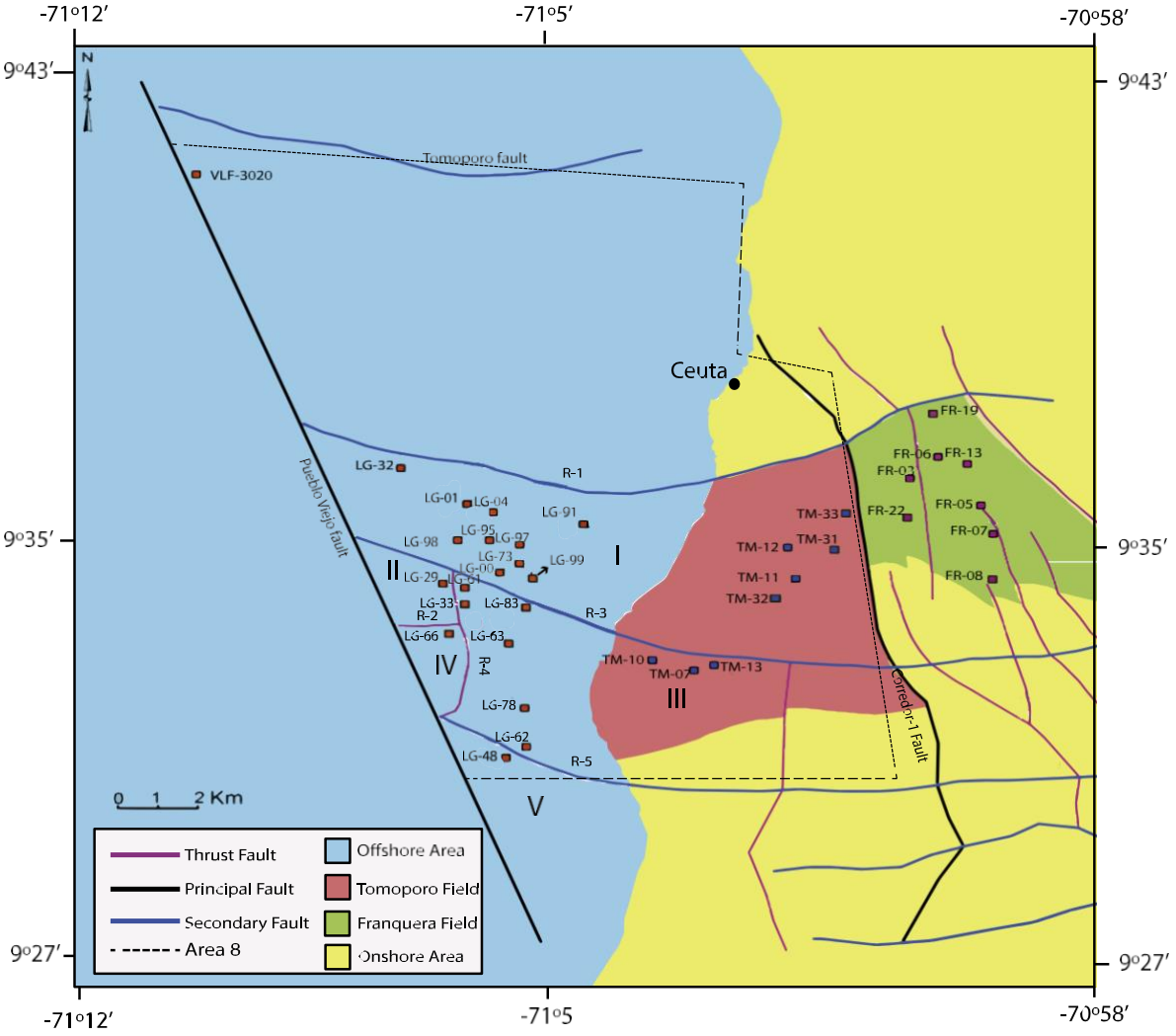

Fig. 2. Structural map of the Ceuta Southeast Area, and situation of the study wells.

3. Samples and methods

First, the 35 oil samples (see Fig. 2) were dehydrated with warm toluene [3]. The API gravity of each sample was measured using a Rice apparatus [4]. The concentrations of V and Ni were determined by inductively coupled plasma atomic emission spectroscopy (ICP-AES) using a Perkin Elmer Optima 3000 sequential spectrometer. The sulfur content was obtained following

the ASTM D4294-10 standard procedure [6] by means of an energydispersive X-ray Panalytical spectrometer (Axios model).

Whole oil gas chromatographic analyses were carried out using a J&W Agilent PONA GC column (50 m x 0.2 mm i.d.; film thickness 0.25 lm; helium was used as carrier gas) in an HP-6890 Series instrument with flame ionization detection (FID). The gas chromatograph operating conditions were as follows: temperature maintained at 35 °C for 15 min, increased from 35 °C to 320 °C at a rate of 2 °C/min, and maintained at 320 °C for 30 min.

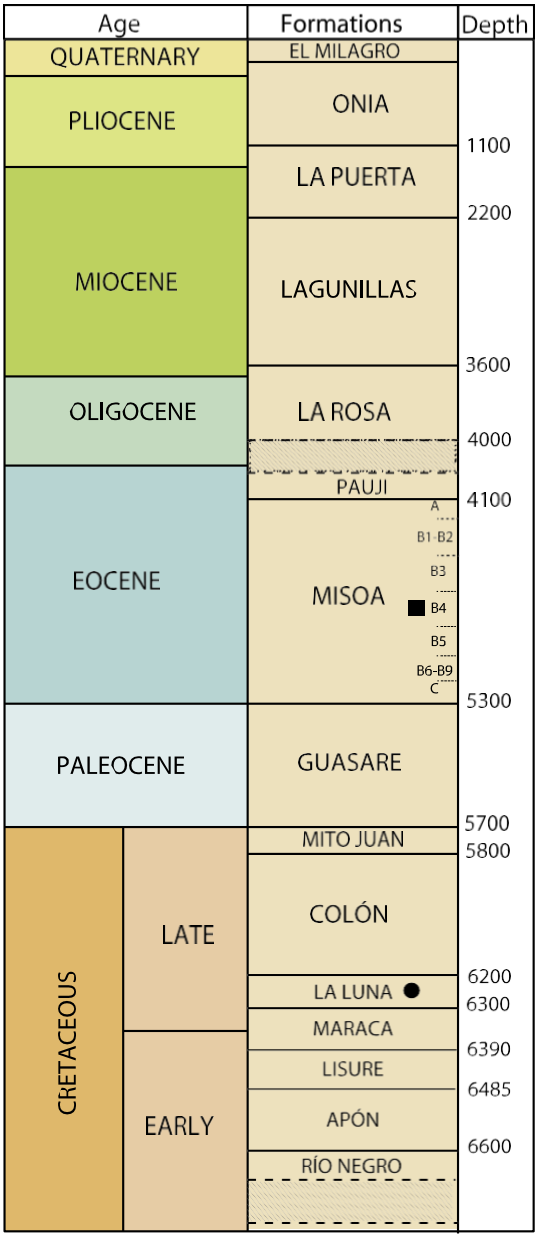

Fig. 3. Stratigraphic column in the Ceuta Southeast Area. Note: source rocks (black circle) and reservoir rocks (black square). Depths are expressed in meters. Nondepositional periods shown by inclined lines.

An aliquot of each sample was fractionated into saturates, aromatics, NSO compounds, and asphaltenes (SARA method [32]. Briefly, asphaltenes were separated with n-heptane in a 1:40 v/v ratio using a Whatman's No. 2 filter paper following the ASTM D3279 standard method [5]. Asphaltenes were then purified several times by Soxhlet extraction with n-heptane until the liquid obtained was colorless. Soluble remnants (maltenes) were then fractionated into saturated hydrocarbons, aromatics, and resins by liquid chromatography [16]. Aliphatic hydrocarbons were eluted with n-hexane, aromatics with toluene, and resins with toluene/methanol (70:30 v/v) using a column filled with silica- alumina. Later, gas chromatography–mass spectrometry (GC–MS) analysis on saturated and aromatic fractions was performed using a HP 5890 Series II gas chromatograph and an Agilent 5973 N mass spectrometer, operating in ''full-scan" mode. Helium was used as carrier gas. An HP-5 column (60 m x 0.32 mm i.d., 0.5-lm film w as also used. The initial oven temperature was 50 °C (held for 2 min), which was ramped at 2.5 °C to reach 300 °C and then held for 70 min. The mass spectrometer was operated in electron ionization mode (EI) at 70 eV. It was calibrated daily under autotuning conditions with perfluorotributylamine (PFTBA), and the chromatograms were acquired in full-scan mode (mass range acquisition was performed from m/z 45 to 500).

Carbon isotopic determination on saturated and aromatic fractions was performed using a Thermo Finnigan 1112 elemental analyzer coupled to a Finnigan Mat Delta C mass spectrometer. The reference materials were USGS 24 graphite, IAEA-CH6 saccharose, IAEA-CH7 polyethylene, and NBS-22 oil. The 13C/12C ratio is reported in ''d" notation and d13C refers to PDB (Pee Dee Belemnite). All analyses were performed in duplicate.

The asphaltene fraction of the LG-62 oil was analyzed using combined flash pyrolysis and gas chromatography with a mass spectrometer detector (Py–GC–MS) in full-scan mode. This analysis was carried out with a Curie-point Pye-Unicam pyrolyser—operated at 700 °C for 8 s intervals—and the same GC–MS instruments were used although operational conditions were modified: 40 °C (initial temperature) and final temperature of 260 °C (held for 16 min). Fourier Transform Infra Red (FTIR) analyses were carried out using a Nicolet 20 SXB apparatus fitted with an arithmetic coprocessor 1240 and a TGS detector. KBr standard pellets were used, and spectra from 4000 to 400 cm-1 were recorded with 64 scans and 2 cm-1 resolution. Preparation of the samples for FTIR analyses and calculation of spectrometric indexes were done following the procedure described by Permanyer et al. [52]. Finally, we also considered previous data [11] referred to the non- degraded single oil from a Cretaceous production well (VLF- 3020) in the Area 8 (see Fig. 2). In regards to statistical treatment of data, a cluster analysis was performed using the SPSS 13.0 pack- age for Windows. The centroid method was applied. The similarity percent was used as grouping parameter [62] and was obtained after calculating Euclidean distances.

4. Results and discussion

4.1. Oil characteristics

4.1.1. Bulk geochemical data

The bulk composition, total sulfur, and API gravities of the 35 oil samples are shown in Table 1. Group type analyses indicated that the Lagotreco and Tomoporo (Area 8 South) samples present similar compositions: the aliphatic-hydrocarbon fraction (SAT) ranged from 30% to 37% (except LG-33 – 47% – and LG-62 – 24%), aromatics in the 30–35% range (excluding LG-33), and a polar fraction (POL) between 27% and 34% (except LG-33 and LG-62 once again, as well as TM-33). The Franquera oils had an almost identical composition: 31–34% of saturated hydrocarbons, as well as slightly low resins plus asphaltenes (26–29%) and high aromatics content (39– 41%) compared to most samples from the other two fields examined. These values are typical of apparently normal crude oils [74]. The API gravity varied from 18° to 20° for the Franquera samples, whereas most samples from (Lagotreco and Tomoporo) showed similar gravities of around 30°. Three ‘‘anomalous” oils (TM-33, LG-62 and LG-33 oils having 23°, 21° and 35°, respectively) have also to be considered apart. High sulfur contents (1.2–2%) were observed in all the samples.

Table 1
Bulk composition, total sulfur content (wt.%), API gravities and d13C values (‰) in whole oil and SARA fractions (wt.%) for the samples.

	SAT	ARO	POL	SAT/ARO	°API	St	$d^{13}C$ $d^{13}C_{RES}$	$d^{13}C_{ARO}$	$d^{13}C_{SAT}$	
FR-03	32	41	27	0.78	19	1.85	−26.63	−26.44	−26.81	−26.67
FR-05	35	39	25	0.88	20	1.79	−26.55	−26.49	−26.71	−26.64
FR-06	34	40	26	0.88	19	1.83	−26.50	−26.50	−26.86	−26.60
FR-07	30	41	29	0.73	18	2.11	−26.48	−26.35	−26.72	−26.68
FR-08	31	42	27	0.74	20	2.04	−26.58	−26.36	−26.84	−26.65
FR-13	33	40	27	0.82	19	1.89	−26.61	−26.43	−26.79	−26.66
FR-19	33	41	26	0.80	19	1.91	−26.53	−26.48	−26.70	−26.62
FR-22	32	40	28	0.80	18	1.94	−26.52	−26.51	−26.88	−26.61
LG-00	36	31	33	1.16	28	1.71	−26.44	−26.33	−26.72	−26.59
LG-01	36	34	30	1.06	28	1.65	−26.51	−26.47	−26.90	−26.50
LG-04	35	31	34	1.13	30	1.80	−26.45	−26.41	−26.70	−26.52
LG-29	35	33	32	1.06	30	1.26	−26.63	−26.33	−26.79	−26.47
LG-32	35	35	30	1.00	28	1.65	−26.66	−26.39	−26.84	−26.59
LG-33	47	27	26	1.74	35	1.22	−26.48	−26.31	−26.79	−26.58
LG-48	35	32	33	1.09	28	1.41	−26.69	−26.45	−26.77	−26.56
LG-61	36	31	33	1.16	30	1.71	−26.66	−26.48	−26.87	−26.61
LG-62	24	34	42	0.71	21	1.39	−26.80	−26.50	−26.90	−26.70
LG-63	34	33	33	1.03	28	1.74	−26.55	−26.35	−26.65	−26.46
LG-66	36	33	31	1.09	30	1.70	−26.49	−26.31	−26.79	−26.63
LG-73	34	34	32	1.00	30	1.79	−26.42	−26.50	−26.89	−26.64
LG-78	37	31	32	1.19	29	1.40	−26.54	−26.31	−26.70	−26.66
LG-83	34	34	32	1.00	30	1.82	−26.42	−26.31	−26.85	−26.69
LG-91	36	31	33	1.16	29	1.74	−26.45	−26.40	−26.85	−26.53

LG-96	34	32	34	1.06	28	1.69	−26.49	−26.48	−26.72	−26.67
LG-97	35	32	33	1.09	29	1.71	−26.50	−26.46	−26.79	−26.58
LG-98	34	34	32	1.00	30	1.67	−26.61	−26.49	−26.79	−26.66
LG-99	34	35	31	0.97	30	1.78	−26.52	−26.45	−26.75	−26.61
TM-07	37	33	30	1.12	29	0.91	−26.69	−26.46	−26.74	−26.46
TM-10	36	34	30	1.06	30	1.84	−26.60	−26.44	−26.69	−26.53
TM-11	34	32	34	1.06	28	1.78	−26.62	−26.41	−26.84	−26.57
TM-12	35	33	32	1.06	30	1.80	−26.57	−26.38	−26.82	−26.46
TM-13	37	36	27	1.03	29	1.81	−26.64	−26.32	−26.80	−26.61
TM-31	36	35	29	1.03	30	1.75	−26.64	−26.42	−26.87	−26.59
TM-32	36	34	30	1.06	29	1.79	−26.56	−26.37	−26.80	−26.45
TM-33	33	34	36	0.99	23	1.76	−26.58	−26.49	−26.80	−26.56
VLF-3020	81	14	5	5.83	42	0.30	–	–	–	–

4.1.2. Carbon isotope results

The similar isotopic compositions of the 35 samples (whole oil, saturates, aromatics, and NSO compounds; see Table 1) suggests that these oils derived from the same source rock; in fact, the standard deviations are close to analytical error (0.5‰). As shown in the Sofer diagram [68] (Fig. 4), d13C values for the oils from the Ceuta Southeast Area indicate a common marine source of organic matter. Although these data must be interpreted with care as biodegradation and maturation may alter the carbon isotopic signature [55], this carbon isotope results do not seem affected by biodegradation and/or maturation degree as reported in similar cases (e.g., [9]).

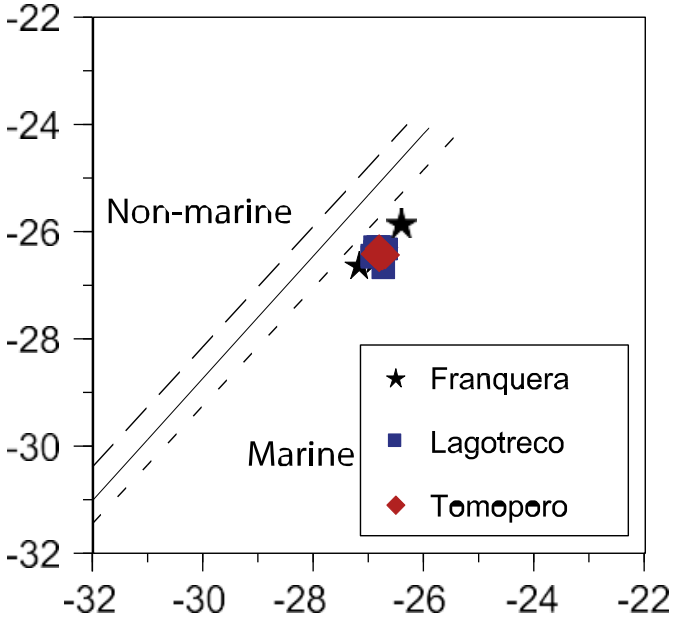

Fig. 4. Sofer isotopes diagram for the Lagotreco, Tomoporo and Franquera aromatic and saturate fractions.

4.2. Biodegradation of oils

Initially, and given the relatively low proportion of saturates and high contents of aromatic and polar compounds in all the samples (see Table 1), these oils may all have undergone biodegradation [27]; for instance the saturate-to-aromatic ratio is below 1 in many samples. In addition, the results of specific gravity (<35° API) also support the notion of biodegradation processes or perhaps the presence of a mixture of a more biodegraded crude oil and unaltered oil which arose as a result of convection or diffusion in the reservoir [45]. This latter hypothesis about mixtures is coherent with the influence of two main events of oil generation and expulsion from the main source rock (La Luna) on the SE area of Lake Maracaibo Basin. These events implied a first charge of oil in the middle Eocene, which was later biodegraded at the end of Eocene after a basin uplift accompanied by an erosive period. Afterwards, a second charge with highly mature fresh non- biodegraded oil took place during the Neogene–Quaternary when the Lake Maracaibo Basin swung S-SE as a consequence of the initial uplift of the Venezuelan Andes [71,25], thereby burying the Misoa B4 reservoir once again. These two generation pulses may explain the presence of low API crude oils in the study area in spite of high API (35° and more) crudes as it could have been expected beforehand. In this regard, whole oil gas chromatography of the samples from Area 8 shows unaltered or slightly altered isoprenoids and a negligible loss of n-alkanes between n-C10 and n- C20 (see Fig. 5a and b).

Moreover, here we introduce the ratios biphenyl vs. triaromatic steroid 28R (BP/TA28R) and norpristane vs. C23 tricyclopolyprenane (norPr/23T) for the first time to compare the relative magnitude of each oil charge in the mixed oils of interest. Notably, the paleobiodegraded oil reached level 6 or higher, according to the Peters and Moldowan scale, as shown by the presence of several 25-norhopanes and the absence of biphenyl or norpristane—the latter two usually degraded at level 5 of the same scale [64,55]. Therefore, on the basis of the observation of norPr/23T and BP/ TA28R ratios close to zero (see Table 2), the LG-62 oil could be considered an almost ‘‘pure” paleobiodegraded end-member. In contrast, the VLF-3020 single oil [11] may represent the unaltered oil charge.

In this case, mixed oils with the highest secondary recharge gave the highest values of the two aforementioned ratios. Therefore, the novel graphical representation of norPr/23T vs. BP/ TA28R shown in Fig. 6 is useful to classify samples into the following two groups: (i) Lagotreco and Tomoporo mixed oils (except TM-33, LG-62 and LG-33, which again are considered ‘‘anomalous” oils); and (ii) samples from the Franquera oilfield.

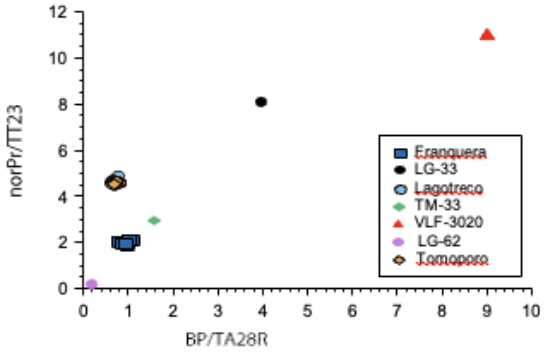

Fig. 6. Plot of norPr/23T against BP/TA28R for studied samples.

Last, the presence of 25-norhopanes in the m/z 177 fragmentograms of the samples (Fig. 7a; peak identifications are in dix A) indicated a heavy level of biodegradation according to the scale defined by Peters et al. [55]. In fact, as previously reported in literature (see [38]; PhD Thesis), the presence of 10- desmethylhopanes in our samples has not been associated with comingled production. Thus, we conclude that paleobiodegraded oil (Eocene pulse) was mixed with unaltered oil (post-Oligocene pulse).

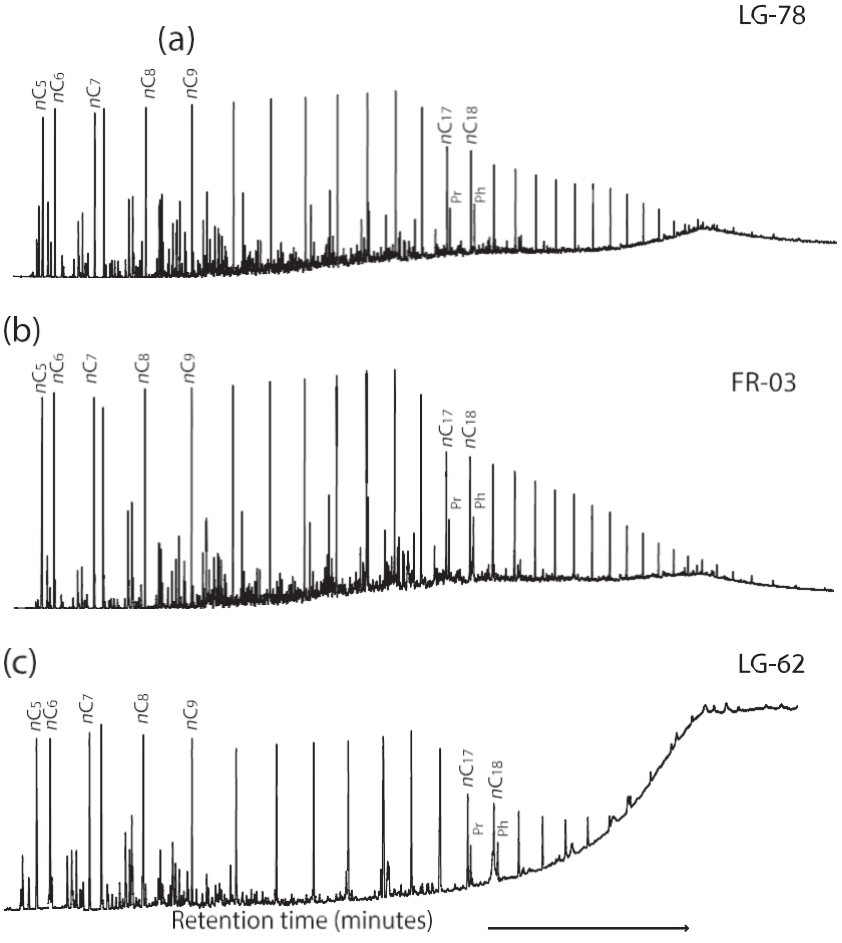

Fig. 5. (a), (b) and (c) Respectively, whole oil gas chromatograms for LG-78, FR-03, and LG-62 samples.

4.3. Depositional environment and organic matter source

High sulfur contents and V/Ni ratios (around 8; see Tables 1 and 2) indicate that all the samples derived from source rocks deposited in a marine carbonate environment under reducing conditions [35]. In fact, during the deposition of carbonate facies, bacterial sulfide is not fully sequestered by iron, and thus nickel ions precipitate in metal sulfides rather than form organometallic compounds. In contrast, stable vanadyl ions show the opposite behavior, leading to high V/Ni ratios [21]. Although V and Ni concentrations can be influenced by petroleum post-accumulation processes, the V/Ni ratio itself tends to be constant as a result of the structural similarities of organometallic compounds that contain these two metals [36]. However, compared to the remaining samples, the TM-07 oil exhibited abnormal V and Ni concentrations, which can be explained by its high clay content [38].

The n-alkane distributions for all the mixed oils were almost identical and typical of marine precursor organic matter [55]: unimodal type with maximum peaks below n-C20 (Fig. 5). Pristane/phytane ratios (Table 2) averaging 0.95 indicate that these samples were generated from organic matter deposited in a marine environment under oxygen-deprived conditions [74]. Although the relative proportions of pristane and phytane are governed by complex processes ([18] and references therein), the Pr/Ph ratio can be used here to indicate the depositional environment. As previously reported by Hunt [31], the Pr/n-C17 and Ph/n-C18 ratios (Table 2) suggest that all the samples can be grouped into the zone that corresponds to oils generated from mature type II kerogen (Fig. 8a). In addition, both the dibenzothiophene/phenanthrene ratio and the total sulfur content (St) are used as paleodepositional–environmen tal indicators of sedimentary rocks [30]. In this context, all our samples were found to lie within the marine carbonate/mixed marine field (Fig. 8b).

Biomarker distributions also denoted a common origin for all the samples. Fig. 7b shows a representative terpanogram of sam ples from Area 8 (peak identifications of terpanes are provided in Appendix A). This m/z 191 mass fragmentogram displays a high relative abundance of the C23 tricyclopolyprenane with respect to the C24 homolog (see Table 2) and other counterparts, thereby pointing to an organic matter source deposited in a carbonate marine environment [55]. Moreover, C26/C25 tricyclopolyprenane ratios of around 0.8 (see Table 2) confirm that the mixed oils were generated from a marine carbonate source rock deposited under anoxic conditions [55]. In these oils, the high abundance of tricyclopolyprenanes can be explained both by a high maturity of the second pulse [77] and by the high degree of biodegradation experienced by the first one [80]. In addition, C31R/C30 hopane ratios exceeding 0.3 (see Table 2) are also indicative of oils deriving from organic matter deposited in a carbonate marine environment under reducing conditions [55]. Furthermore, all the samples showed 18a(H)-22,29,30 trisnorneohopane/17a(H)-22,29,30 tris- norhopane ratios (Ts/Tm) lower than 1 (see Table 2), indicating again that these samples were derived from a carbonate source rock deposited in a reducing environment [65]. Finally, given the preceding results and the fact that the marine-origin oils of the Lake Maracaibo

Basin commonly lack oleanane (e.g., [71], the presence of this non-hopanoid triterpene in our samples is inconclusive and could be explained by an exogenous input during petroleum migration and accumulation in the Misoa B4 reservoir [54]. However, the interference of 25-norhomopanes cannot be ruled out [1]. Fig. 9 presents a representative m/z 217 fragmentogram of saturates (peak identifications of steranes are provided in Appendix A). The high abundance of C27 regular steranes compared to the C28 and C29 homologs indicates a marine carbonate source rock [66]. Such a source facies for our mixed oils is also denoted by the low values (<0.26) of the diasteranes/regular steranes ratio (see Table 2).

Table 2
Geochemical indicators of source depositional environment for saturates and aromatics in samples from the Ceuta Southeast Area.

	BP/TA28R	norPr/23T	Ts/Tm	Pr/Ph	V/Ni	V	Pr/*n*-C_{17}	Ph/*n*-C_{18}	26/25T	24/23T	DBT/P	Dia/ST	31R/30H
FR-03	1.00	2.00	0.50	0.93	7.66	349.74	0.31	0.44	0.76	0.47	0.71	0.22	0.37
FR-05	1.00	1.90	0.51	0.93	7.86	325.46	0.40	0.42	0.73	0.42	0.71	0.22	0.43
FR-06	1.00	1.90	0.49	1.00	7.68	337.73	0.32	0.45	0.78	0.43	0.70	0.22	0.42
FR-07	0.80	2.00	0.50	0.98	7.69	411.04	0.41	0.41	0.79	0.49	0.70	0.23	0.38
FR-08	1.10	2.10	0.52	0.94	7.78	394.04	0.40	0.50	0.82	0.46	0.71	0.25	0.45
FR-13	0.90	1.95	0.48	0.91	7.36	353.63	0.38	0.42	0.80	0.46	0.73	0.20	0.40
FR-19	1.05	2.05	0.51	0.93	7.46	339.34	0.39	0.47	0.87	0.45	0.74	0.20	0.38
FR-22	0.95	1.95	0.47	0.91	7.58	381.47	0.36	0.45	0.86	0.45	0.73	0.21	0.40
LG-00	2.46	4.56	0.47	0.97	8.30	342.00	0.35	0.48	0.81	0.43	0.93	0.23	0.42
LG-01	2.50	4.59	0.49	0.96	8.51	304.84	0.34	0.42	0.78	0.50	0.90	0.23	0.38
LG-04	2.57	4.41	0.48	0.96	9.24	306.75	0.34	0.43	0.85	0.42	0.91	0.23	0.42
LG-29	2.59	4.42	0.48	0.96	7.10	236.26	0.32	0.42	0.76	0.48	0.91	0.24	0.41
LG-32	2.46	4.54	0.48	0.93	8.54	296.64	0.33	0.40	0.88	0.47	0.91	0.25	0.41
LG-33	4.00	8.00	0.55	0.90	8.70	151.99	0.31	0.48	0.78	0.40	1.01	0.25	0.45
LG-48	2.58	4.48	0.48	0.97	8.06	273.04	0.31	0.45	0.72	0.41	0.91	0.24	0.40
LG-61	2.58	4.50	0.48	0.98	8.48	285.96	0.38	0.48	0.79	0.45	0.90	0.25	0.41
LG-62	0.20	0.10	0.38	0.98	7.18	337.99	0.34	0.43	0.83	0.43	0.80	0.23	0.43
LG-63	2.45	4.42	0.49	0.98	8.51	337.90	0.40	0.43	0.82	0.43	0.92	0.20	0.42
LG-66	2.52	4.49	0.49	0.94	8.59	299.12	0.36	0.42	0.81	0.46	0.92	0.21	0.43
LG-73	2.48	4.43	0.47	0.94	8.40	363.21	0.36	0.47	0.74	0.41	0.92	0.25	0.44
LG-78	2.50	4.50	0.48	0.93	7.45	247.36	0.34	0.44	0.81	0.50	0.90	0.23	0.38
LG-83	2.57	4.42	0.49	0.98	8.52	372.73	0.40	0.47	0.79	0.44	0.91	0.24	0.45
LG-91	2.41	4.57	0.47	0.95	8.41	317.38	0.40	0.46	0.80	0.45	0.91	0.20	0.38
LG-96	2.47	4.43	0.49	0.95	8.25	357.73	0.35	0.50	0.79	0.48	0.93	0.22	0.43
LG-97	2.50	4.52	0.48	0.95	8.33	338.18	0.40	0.41	0.80	0.50	0.92	0.21	0.42
LG-98	2.48	4.41	0.48	0.96	8.43	333.41	0.41	0.42	0.79	0.42	0.89	0.22	0.42
LG-99	2.51	4.43	0.49	0.96	8.33	381.92	0.35	0.49	0.84	0.45	0.91	0.22	0.42
TM-07	2.59	4.47	0.47	0.96	7.37	142.15	0.38	0.41	0.71	0.42	0.92	0.21	0.44
TM-10	2.50	4.45	0.47	0.98	7.48	325.47	0.36	0.43	0.82	0.48	0.90	0.23	0.43
TM-11	2.45	4.57	0.49	0.93	7.46	339.50	0.38	0.46	0.80	0.47	0.91	0.24	0.42
TM-12	2.49	4.48	0.49	0.99	7.40	326.72	0.33	0.43	0.78	0.48	0.91	0.21	0.44
TM-13	2.48	4.41	0.49	0.96	7.58	329.74	0.39	0.48	0.75	0.44	0.92	0.21	0.45
TM-31	2.51	4.55	0.46	0.94	7.71	263.68	0.37	0.47	0.82	0.45	0.83	0.20	0.42
TM-32	2.46	4.39	0.47	1.00	8.05	350.65	0.38	0.44	0.85	0.46	0.88	0.20	0.43

TM-33	1.60	2.90	0.46	0.99	7.61	334.80	0.31	0.41	0.77	0.44	0.77	0.22	0.41
VLF-3020	9.00	11.00	0.63	1.00	8.15	–	0.31	0.39	0.80	0.40	1.27	0.20	–

Notes: V contents expressed in ppm; BP/TA28R = Biphenyl to C_{28} 20R triaromatic steroid; Ts/Tm = 18a(H)-22,29,30 trisnorneohopane/17a(H)-22,29,30 trisnorhopane; Dia/ ST = diasterane ratio; norPr/23T = norpristane to C_{23}-tricyclopoliprenane; DBT/P = dibenzothiophene/phenanthene; and 26/25T = C_{26}-tricyclic terpanes/C_{25}-tricyclic terpane.

The relative abundance of the methyldibenzothiophene isomers (MDBT) in all the mixed oils varied in the following order: 4 > 2 +3 ~ 1 (Fig. 10a and b, peak identifications of aromatics are in Appendix A). Thus, neither sample clearly showed the usual distribution pattern for the MDBT homologs corresponding to the carbonate lithology, with the co-eluting isomers (2and 3-methyl) being the least abundant [29]. Although alternative explanations for this MDBT pattern cannot be dismissed, the most probable scenario requires a parallel 4-/1-MDBT rise with increasing maturation [57]. Otherwise, additional explanations include a lateral change in source-rock lithology [19] and/or selective water washing of the MDBT isomers [24].

4.4. Thermal maturity

Several molecular maturation parameters (bishomohopane isomerization ratio, methylphenanthrene index, and sterane isomerization ratios; among others) for saturated and aromatic fractions separated from the samples are listed in Table 3. Nevertheless, it must be pointed out that these parameters (perhaps with the only exception of the methylphenanthrene ratio) could not be applicable given the previously established mixture of a palaeobiodegraded oil charge (Eocene) and the fresh oil charge (postOligocene); that is to say, regular steranes, triterpanes, and triaromatic steroids were not fully removed in the first biodegraded oil [55].
The bishomohopane isomerization ratios (%22S) showed an average value of 0.59 (Table 3), therefore all the samples reached the equilibrium stage (vitrinite reflectances exceeding 0.6%; [41]

The sterane isomerization ratios (%20S and %bb; see Table 3) rose from 0 to 0.55 and from 0–0.5 to 0.7, respectively, with increasing thermal maturity [55]. Most of the mixed oils (except LG-62) showed %20S and %bb ratios averaging about 50%, which would be indicative of a thermal maturity level equivalent to the onset of peak oil generation. In contrast, LG-62 oil displayed lower % 20S and %bb values (43%) than the other samples. Assuming that the LG-62 oil has a very low charge of post-Oligocene fresh unaltered oil, the latter values support a maturation level equivalent to 0.63% within the early oil window [31] and very close to the Eocene oil generation pulse. Also, all the samples showed %20S and %bb ratios with a strong positive linear correlation, suggesting vertical migration through faults rather than ‘‘geochromatograph y” during migration in the study area [55]. This observation is in accordance with the literature [71].

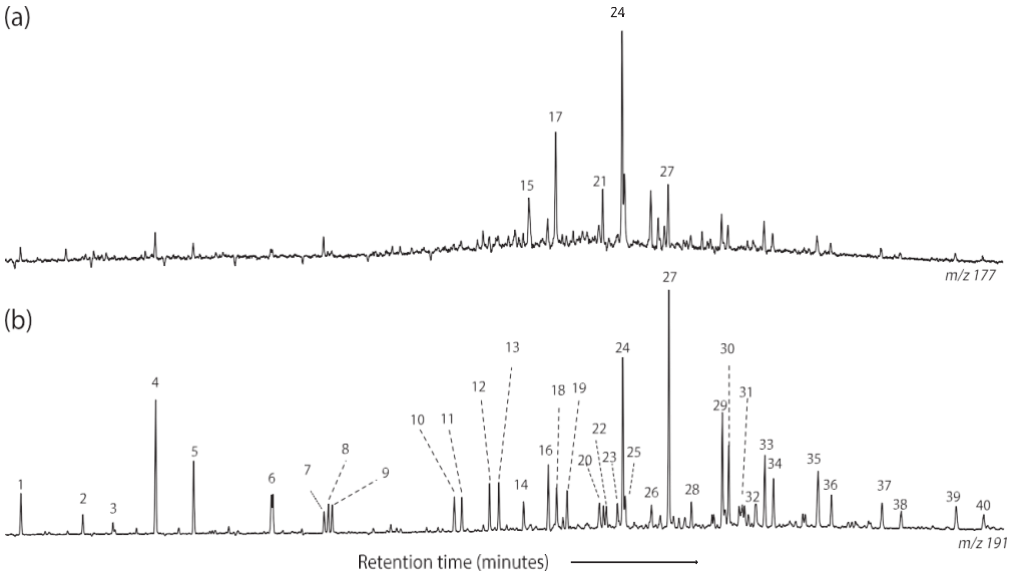

Fig. 7. (a) and (b) Respectively, m/z 177 and m/z 191 ion fragmentograms showing 25-norhopane and terpane distributions for the characteristic LG-78 sample.

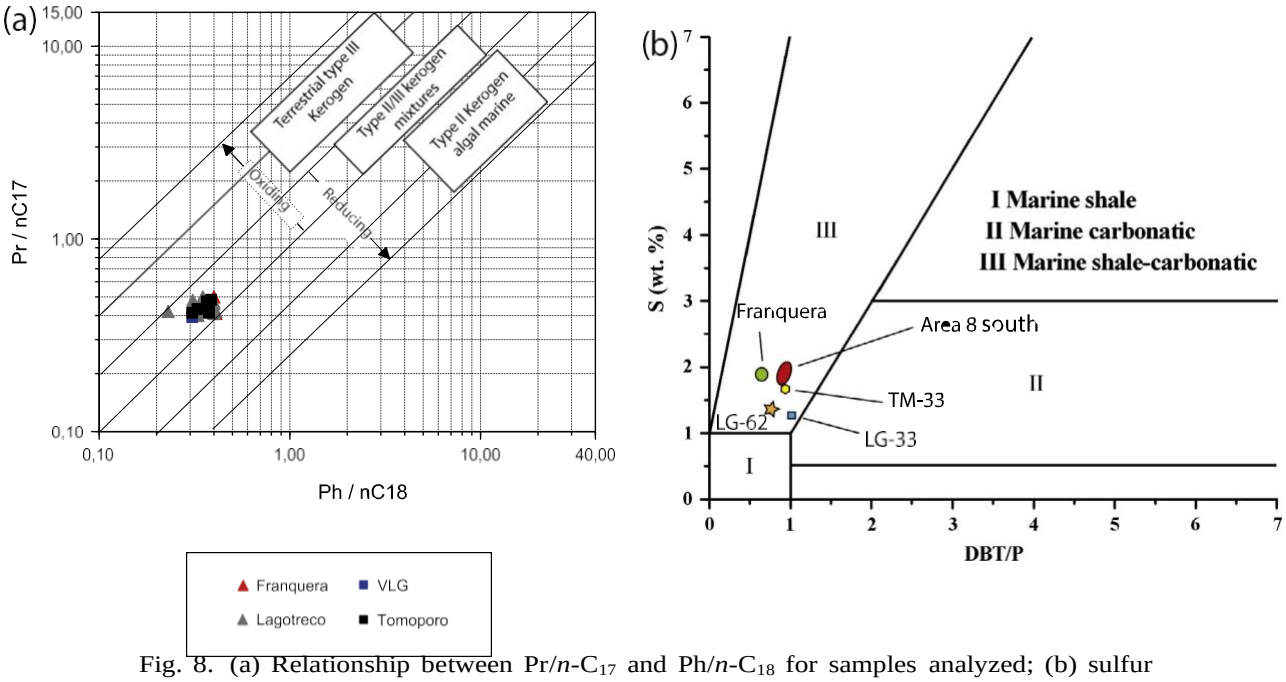

Fig. 8. (a) Relationship between Pr/*n*-C_{17} and Ph/*n*-C_{18} for samples analyzed; (b) sulfur content (% wt.) versus DBT/P. Note: I (marine shales), II (marine carbonates) and III (marine carbonates/marine mix).

The characteristic triaromatic (TA) steroid peaks were identified in the m/z 231 fragmentograms for the samples from the Ceuta Southeast Area (Fig. 11a). According to Peters et al. [55], an useful maturity parameter (the TA ratio; see Table 3) has been applied in this case. Variations in the values of this ratio between most of the samples were relatively small (see Table 3). Most of the mixed oils showed similar values (about 0.4), thus corroborating the presence of mature oils in

the Misoa B4 reservoir; however, LG-62 and LG-33 samples showed distinctive values (0.31 and 0.51), indicating lower and higher maturation levels (%Rc1 about 0.63% and 0.82%), respectively, when compared to the other samples.

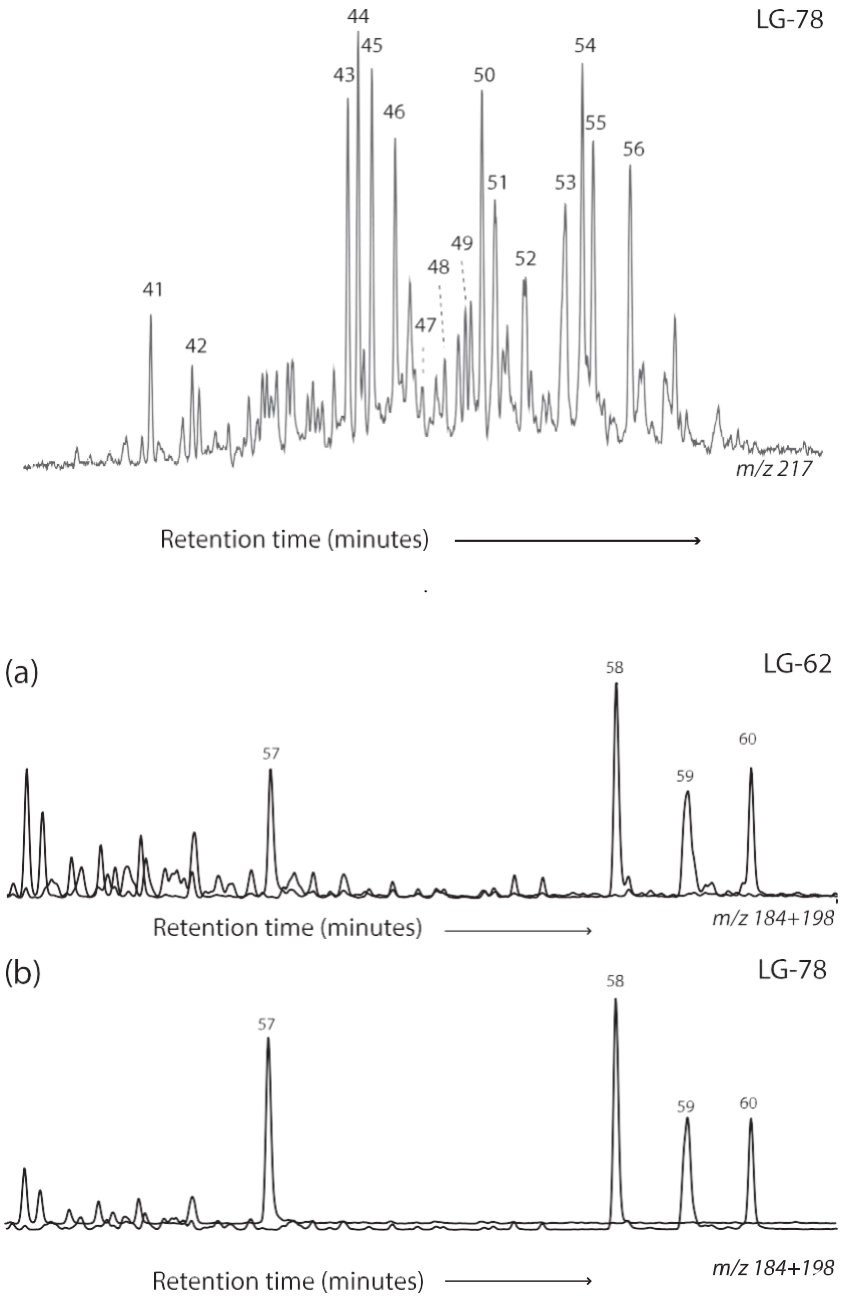

Fig. 9. Example of m/z 217 ion fragmentogram showing sterane distribution for the representative LG-78 sample

With respect to the methylphenanthrene ratio (MPR or ratio of 2- vs. 1-methylphenanthrene), this measurement is a valid indicator of the maturation level of marine organic matter only at vitrinite reflectances of around 0.9 [59,13]. In our case, all the samples showed very similar MPR values (1.18 on average; see Table 3), indicating a common maturity level equivalent to 0.93%. The almost identical MPR values can be explained by the higher susceptibility of 1- and 2-

methylphenanthrene to biodegradation than the other two isomers [8]. Consequently, both 1- and 2- isomers would have been removed from the palaeobiodegraded first pulse (Eocene) prior to the appearance of the 25-norhopanes [78]. Thus the ratio could define with precision the maturity of the second pulse (Neogene–Quaternary). Moreover, this latter maturity level is coherent with that of VLF-3020 oil (MPR of ~1.2). These data, the other maturity parameters of the VLF-3020 sample (see Table 3), and the fact that our samples and this latter oil (see bulk geochemical and biomarker data in Tables 1 and 2) derived from the same carbonate source rock (La Luna), lead us to tentatively propose that VLF-3020 represents the end-member of an unaltered contribution. We also calculated the methylphenanthrene index values (MPI- 1; [60,58]) for the mixed oils. These showed mostly MPI-1 values about 0.8 and therefore calculated vitrinite reflectances (%Rc2) ranging from 0.77% to 0.83% (see Table 3 and Fig. 11b). These val- ues denote maturation levels just before the peak of the oil window and they are slightly lower than those of the post-Oligocene oil charge (calculated vitrinite reflectance of ~0.93%). This latter observation is consistent with the predominance of 9- methylphenanthrene over the other three less recalcitrant homologs in the paleobiodegraded Eocene oil [28]. Thus, as expected, the LG-62 sample displayed an abnormally low MPI-1 value of 0.55 (%Rc2 equal to 0.73%) when compared to the remaining samples. Last, the dominance of Tm over Ts (see Table 2) may also indicate that the carbonate source rocks which generated the mixed oils of interest were thermally mature [67]. In this regard, the Ts- to-Tm ratio decreased in the following order: VLF-3020 > LG- 33 > Area 8 South > TM-33 > Franquera > LG-62, which is consistent with the results obtained from the novel graph of norPr/23T against BP/TA28R (Fig. 6).

Table 3
Maturity-related molecular parameters for the saturates and aromatics in sampled crude oils from the Ceuta Southeast Area.

	%22S	%20S	%bb	MPR	TA	Rc_1	MPI-1	Rc_2
FR-03	56	48	51	1.13	0.42	0.76	0.77	0.86
FR-05	56	47	49	1.15	0.41	0.77	0.77	0.86
FR-06	59	48	50	1.19	0.42	0.76	0.78	0.87
FR-07	56	49	51	1.14	0.41	0.75	0.79	0.87
FR-08	59	46	49	1.18	0.41	0.76	0.79	0.87
FR-13	58	47	50	1.13	0.42	0.76	0.77	0.86
FR-19	57	48	50	1.12	0.40	0.75	0.76	0.85
FR-22	58	47	49	1.16	0.41	0.78	0.78	0.87
LG-00	58	49	52	1.19	0.48	0.78	0.81	0.88
LG-01	58	47	50	1.18	0.47	0.79	0.81	0.88
LG-04	60	47	49	1.17	0.46	0.77	0.80	0.88
LG-29	60	49	51	1.17	0.48	0.78	0.80	0.88
LG-32	58	48	49	1.18	0.49	0.78	0.79	0.87
LG-33	60	51	57	1.16	0.54	0.82	0.82	0.89
LG-48	58	46	49	1.17	0.46	0.80	0.79	0.87
LG-61	56	46	50	1.18	0.48	0.78	0.80	0.88
LG-62	59	43	43	1.15	0.31	0.63	0.55	0.73
LG-63	59	49	51	1.19	0.47	0.79	0.79	0.87
LG-66	56	47	50	1.18	0.48	0.78	0.79	0.88
LG-73	57	47	51	1.18	0.47	0.79	0.80	0.88

LG-78	59	48	51	1.18	0.47	0.78	0.80	0.88
LG-83	57	46	48	1.18	0.47	0.79	0.79	0.87
LG-91	56	48	51	1.18	0.49	0.77	0.80	0.88
LG-96	57	49	52	1.18	0.46	0.78	0.80	0.88
LG-97	56	47	50	1.18	0.47	0.78	0.79	0.87
LG-98	59	47	50	1.18	0.47	0.79	0.79	0.87
LG-99	60	48	51	1.17	0.47	0.79	0.80	0.88
TM-07	60	49	52	1.17	0.47	0.78	0.81	0.88
TM-10	58	48	50	1.18	0.46	0.77	0.81	0.88
TM-11	59	49	51	1.19	0.48	0.78	0.79	0.88
TM-12	56	48	51	1.19	0.49	0.79	0.78	0.87
TM-13	59	46	49	1.18	0.47	0.77	0.81	0.89
TM-31	58	47	50	1.14	0.48	0.78	0.79	0.88
TM-32	57	47	49	1.16	0.47	0.78	0.80	0.89
TM-33	60	49	52	1.20	0.45	0.77	0.78	0.86
VLF-3020	60	56	69	1.20	0.80	0.92	0.90	0.94

Notes: %22S or 22S/(22S + 22R) = 17α,21b(H)-29-bishomohopane ratio (%); %bb = (20R + 20S)C_{29}αbb sterane ratio (%); %20S = 5α,14α,17α(H)-stigmastane 20S and 20R ratio (%); TA = C_{20} homologue to C_{20} plus C_{28} 20R triaromatic steroid hydrocarbon ratio; vitrinite reflectance from MPR equal to 0.94 + 0.99-log-MPR [59]; Rc_1 = 0.37 + 0.7-TA in accordance with Mackenzie et al. [42]; MPI-1 = 1.5-(2-MP + 3- MP)/(P + 1-MP + 9-MP); Rc_2 = 0.4 + 0.6-MPI-1, assuming Ro_2 in the 0.65–1.35

4.5. Asphaltene pyrolysis

Ion chromatograms for m/z 57, 142, 156, 178, 184, 192, and 198 corresponding to the LG-62 sample obtained after asphaltene separation and its Py–GC/MS are shown in Fig. 12. Note a high proportion of the low-chain n-alkanes ranging between n-C8 and n-C14, typical of crude oils deriving from source rocks of marine organic matter [55]. The lower abundance of methyldibenzothiophenes with the co-eluting isomers (2- and 3-methyl), as well as DBT/P and Pr/Ph values of about 1 and 1.3, suggest a carbonate source rock deposited under oxygen-deprived conditions [29,30]. Other Py–GC/MS results, such as the predominance of 2-ethyl and 2-methylnaphthalene homologs over their respective isomers and the 4-/1-MDBT ratio slightly higher than unity, indicate that the pyrolysate and the LG-62 oil have approximately the same maturity levels (~0.6%) in the early part of the oil window [57,55]. This feature is coherent with the fact that the LG-62 oil can be considered an almost ‘‘pure” paleobiodegraded end-member. In addition, the pyrolysate showed an abnormal MPI-1 index value of 0.65 (% Rc2 of 0.79%), thereby corroborating that the MPI-1 index is not a useful maturity parameter for early mature oils derived from La Luna source rocks [13].

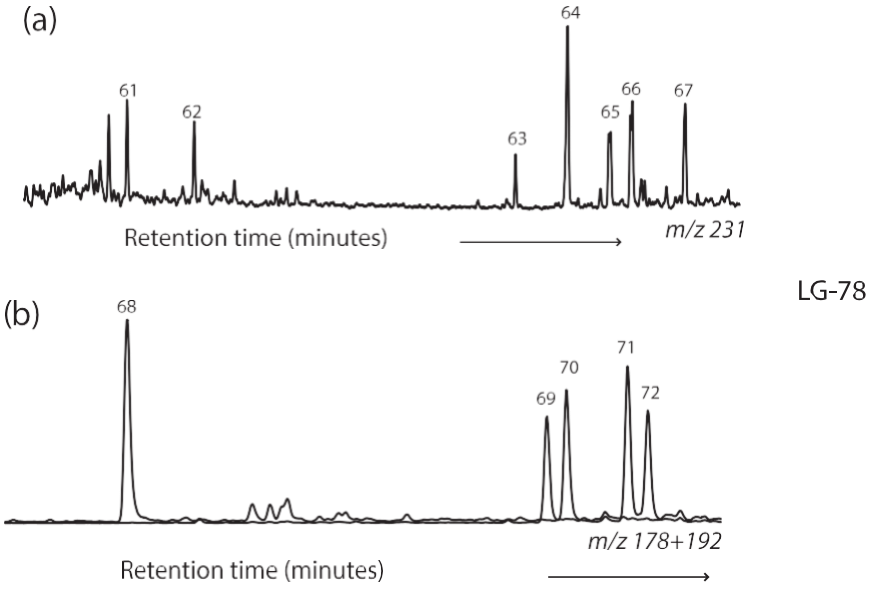

Fig. 11. (a) and (b) Respectively, m/z 231 and m/z 178 + 192 ion fragmentograms showing triaromatic steroids and for methylphenanthrene derivates for the representative LG-78 sample.

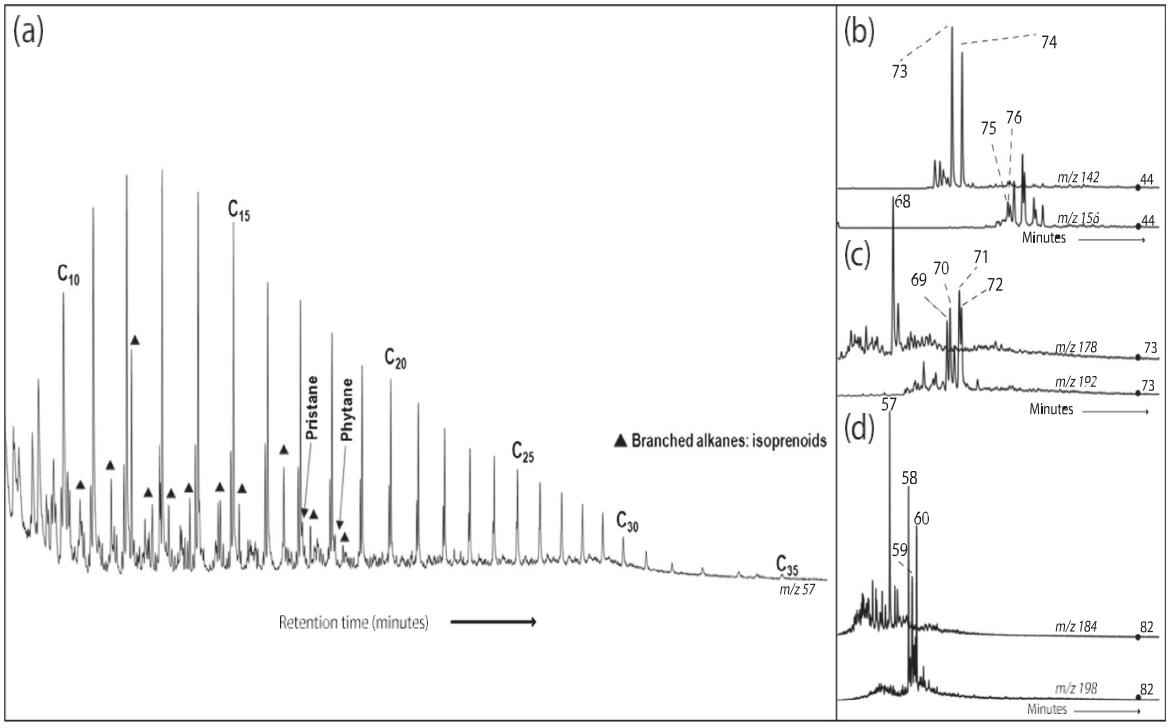

Fig. 12. (a), (b), (c) and (d) Respectively, distribution patterns of the paraffin hydrocarbons, naphthalene series, phenanthrene compounds, and dibenzothiophenes for the product obtained by pyrolysis of the LG-62 sample.

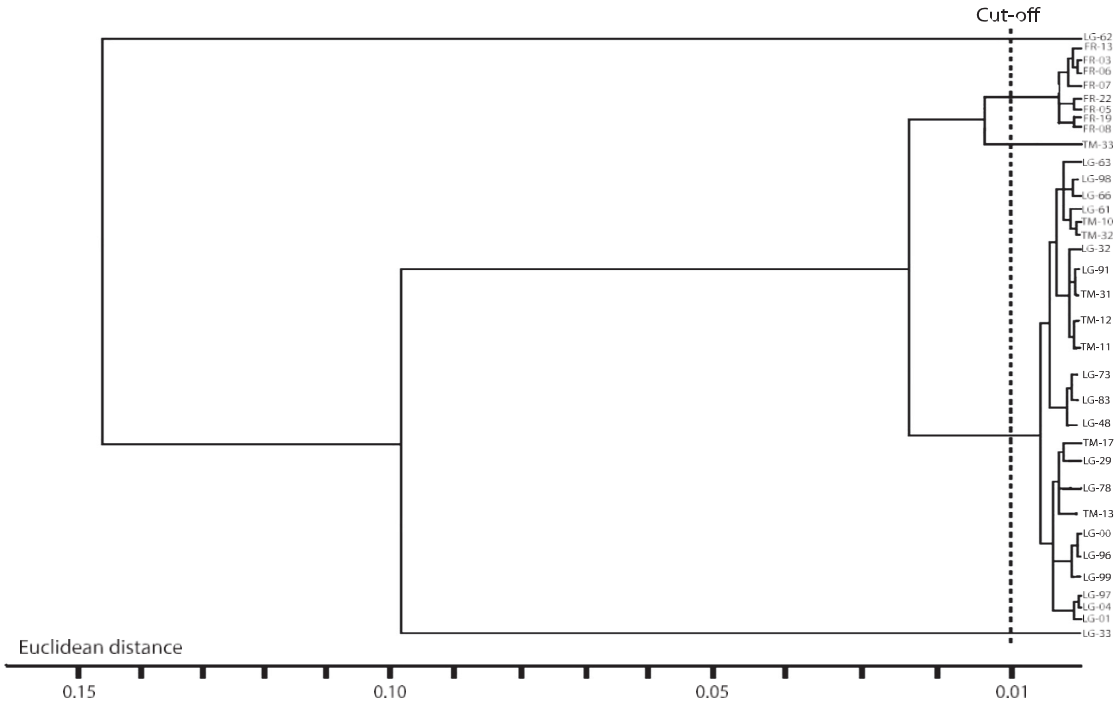

Fig. 13. Dendrogram showing the clustering of sampling wells.

4.6. Geochemical correlations

In an attempt to establish the La Luna Formation as the source rock for the oils from Area 8, we compared the geochemical data of our samples with those previously reported for several La Luna rock extracts from the southeastern coast of Lake Maracaibo [71,46]. Thus, taking into account the high sulfur content and V/ Ni, the d13C values of oils derived from Cretaceous source rocks, the lack or near-absence of oleanane, as well as the distribution of steranes (C27 > C28 > C29) and tricyclopolyprenanes (prevalence of C23 tricyclic terpane over other homologs), we conclude that the La Luna rocks correlate very well with the mixed oils sampled. To classify all the oil samples into one or various families, we conducted multivariate statistical analysis based on 20 variables Pr/Ph, Pr/n-C17, Ph/n-C18, 22/21T, 24/23T, Ts/Tm, DBT/P, %22S, MPR, MPI-1, TA ratio, %bb, %20S, diasterane ratio, %SAT, %ARO, SAT/ARO, °API, %St, and V/Ni) by means of hierarchical clustering. The dendrogram plot in Fig. 13 shows two clusters (Area 8 South and Franquera) and it was obtained from our experimental data. As expected, measurements of similarity within the family formed by all the Franquera samples corroborate their high similarity (cutoff of 0.01 in terms of Euclidean distance) using the proximity procedure [22]. Mixed oils from Area 8 South (excluding the ‘‘anomalous” oils: TM-33, LG-62, and LG-33) also showed high similarity.

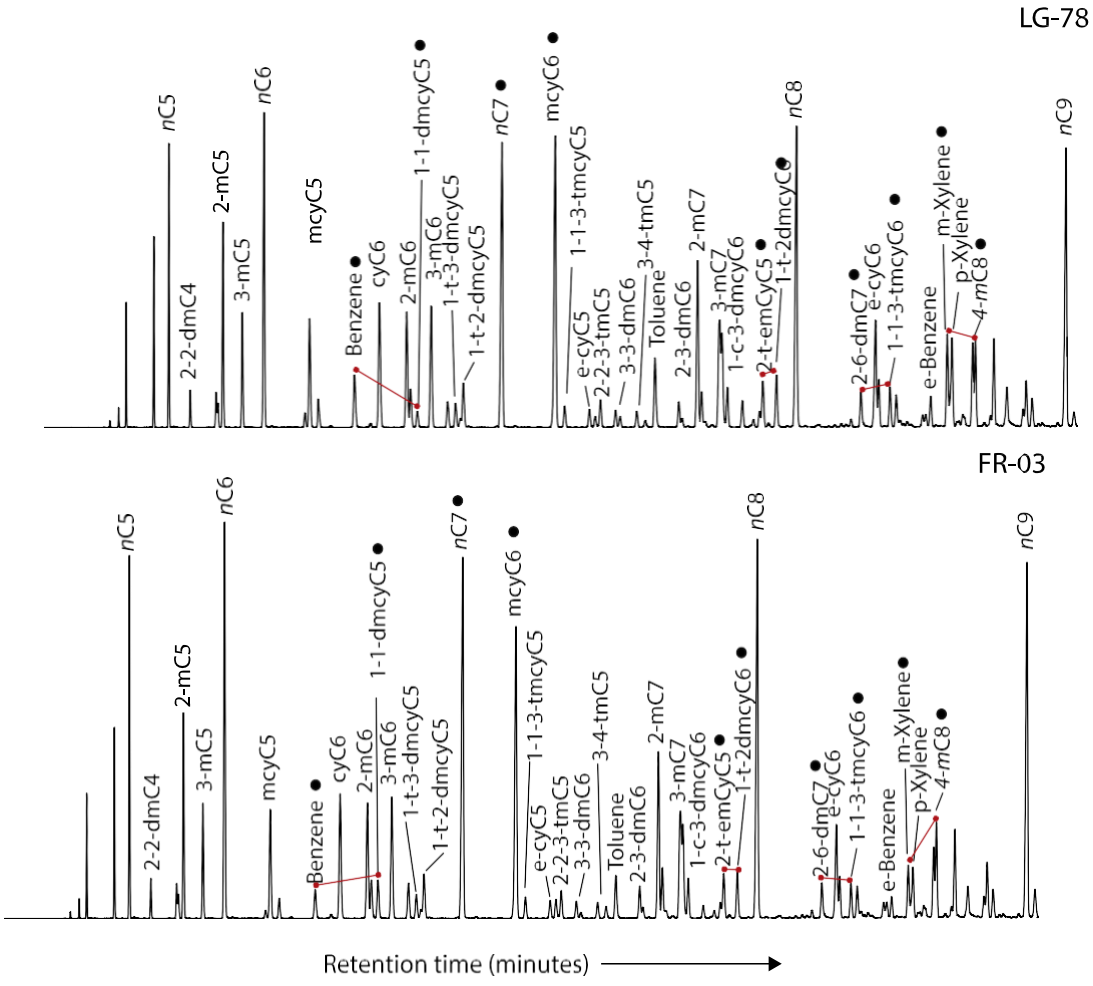

Fig. 14. Gas chromatogram fingerprints from n-C5 to n-C9 for representative FR-03 and LG-78 oils showing the peaks selected to calculate all the ratios A to F plotted on star diagrams.

4.7. Reservoir continuity within the Misoa B4 unit in the Ceuta Southeast Area

As previously mentioned, Area 8 can be divided into at least six blocks (Area 8 South I to V and Franquera; see Fig. 2) on the basis of structural features. Although all the mixed oils from this area are of the same origin (La Luna source rock), some of them presented distinctive API gravities and compositional differences (Tables 1–3). Assuming that such variations in the samples could be partly explained by fault compartmentalization of the Misoa B4 reservoir and the relative amounts of oil accumulated during the Eocene and post-Oligocene generation pulses, several petroleum postaccumulation processes cannot be dismissed at 150 °C [56]. The light hydrocarbon distributions were examined for the mixed oils sampled from Area 8, following the method proposed by Kaufman et al. [33]. Fig. 14 shows the n-C5 to n-C9 gas chromatograms for two representative samples (LG-78 and FR-03). In this case, the different toluene/n-C7 values (higher and lower than 0.2, respectively) and n-C7/methylcyclohexane values (inferior and superior to 1) for samples LG-78 and FR-03 may indicate that water solubilization processes have

a significant influence on Franquera API gravities [73]. Contrary to what might be expected given the lower relative magnitude of the Eocene oil in the mixed oils from the Franquera field compared to the LG-62 sample (see Fig. 6), the latter showed a slightly higher API gravity value (21°) than those for the Franquera mixed oils (620°). This higher value might be attributable to the solubilization of petroleum components in water [49].

We compared the whole oil gas chromatograms and selected six minor inter paraffin peak ratios in the region from n-C5 to n-C9. Some of these parameters cover the maximum difference of the peak ratios of the oil pool in our wells, others indicate water solubilization, and they all can truly reflect the continuity of the fluid of Misoa B4 reservoir in the sector under study. Therefore, they were plotted on star diagrams to establish similarities or dissimilarities between the mixed oils (Fig. 15).

The star diagrams shows the two main oil families related to Misoa B4 reservoir allocations. The first group comprises oils from Area 8 South, while all the Franquera mixed oils form the second family. The Corredor 1 fault acts as a seal between two separate reservoir compartments, impeding any communication between them. This observation contrasts with other faults (see Fig. 2) that favor reservoir continuity within the Lagotreco and Tomoporo fields. These results are in accordance with variations in the geochemical data for most of the samples. Moreover, the star diagrams of the ‘‘anomalous” oils (TM-33, LG-62, and LG-33) presented large similarities between them and with the other samples from Area 8South. This observation is in disagreement with the notion that several molecular parameters and bulk geochemical properties for these three mixed oils clearly differ from one another and from those of the remaining samples from Area 8 South (for instance, 23°, 21°, 35°, and 28° – on average – API gravities). This contradiction could be explained by the similar chromatographic fingerprints for the mixed oils from Area 8 South being fundamentally assigned to the secondary recharge. As in other case studies (see [53]), gas chromatography fingerprints would have failed to identify reservoir discontinuities within the Lagotreco and Tomoporo fields. Thus we used an alternative tool, namely the FTIR method described by Permanyer et al. [52], in order to provide evidence of compartmentalization within the Misoa B4 reservoir rock in the sector under study.

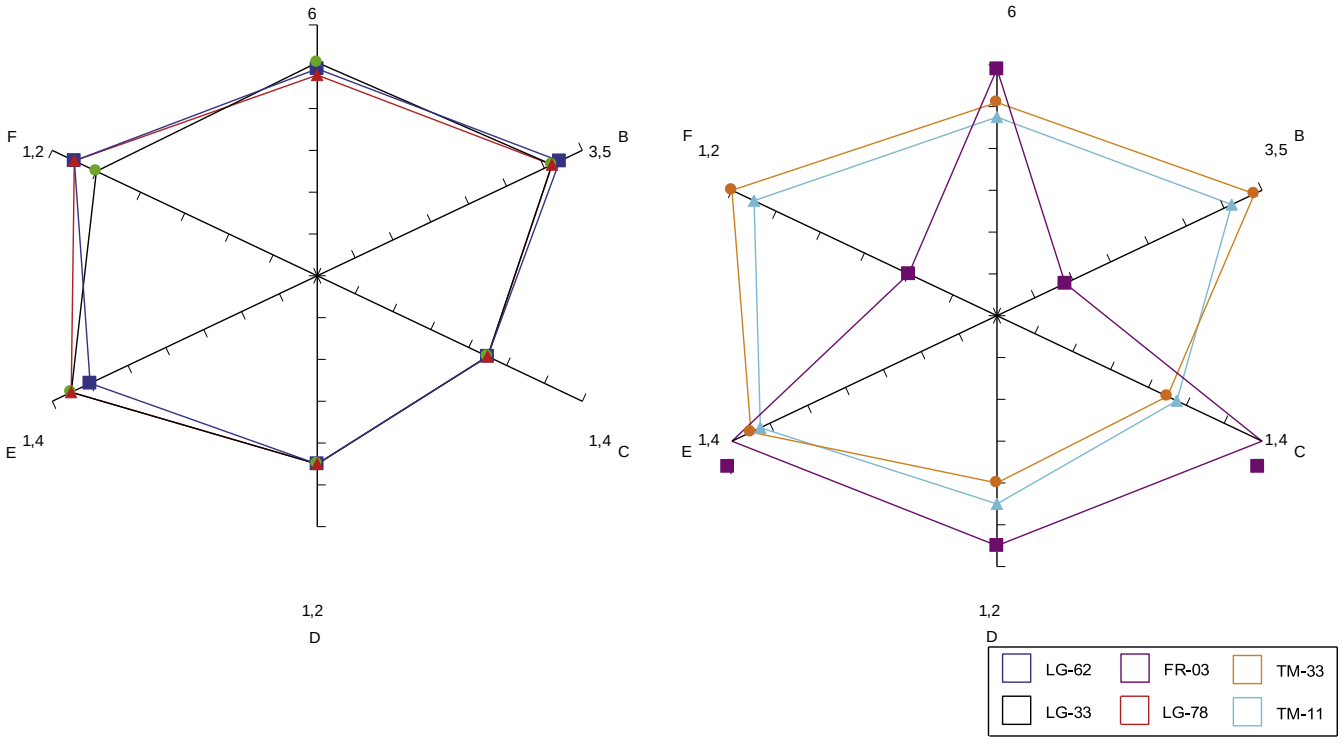

Fig. 15. Star diagrams of the samples FR-03, LG-78, LG-33, LG-62, TM-11 and TM-33. Note the use of the six pairs of components (A to F) in the order given: n-heptane to toluene ratio, benzene to 1,1-dimethylcyclopentane, n-heptane to methylcyclohexane, 2t-ethylmethylcyclopentane to 1t,2-dimethylcyclohexane, 2,6-dimethylheptane to 1,1,3-trimethylcyclohexane, as well as m-xylene to 4-methyloctane.

Last, we also applied FTIR spectroscopy to the 35 samples using indices previously reported in the literature [26]. Assignments of the FTIR bands were determined by reference to earlier studies (e.g., [51]. The aliphaticity, long chains, aromaticity and branched indices proved to be the most appropriate features to distinguish the mixed oils analyzed. Thus, the LG-33 and LG-62 samples showed the lowest and highest aliphaticity and aromaticity values, respectively, when compared to the other samples from Area 8 South (Fig. 16a). However, this diagram does not clearly differentiate between the mixed oils from each side of the Corredor 1 fault. In contrast, the results from a comparison of the long chains vs. branched indices (Fig. 16b) appear to be more accurate to determine reservoir continuity, with five groups of samples being clearly defined. Oil samples from the Franquera field and Area 8 South (except LG-33, LG-62, and TM-33), respectively, form two homogeneous groups of mixed oils related to compartments separated by the Corredor 1 fault. These two families are coherent with those determined by the gas chromatographic fingerprint method. Finally, the LG-33, LG-62, and TM-33 mixed oils each constitute a roup, thereby indicating the existence of permeability baffles and barriers within the Misoa B4 reservoir rock in Blocks I and III, with no connectivity between these three wells and the other wells in Area 8 South.

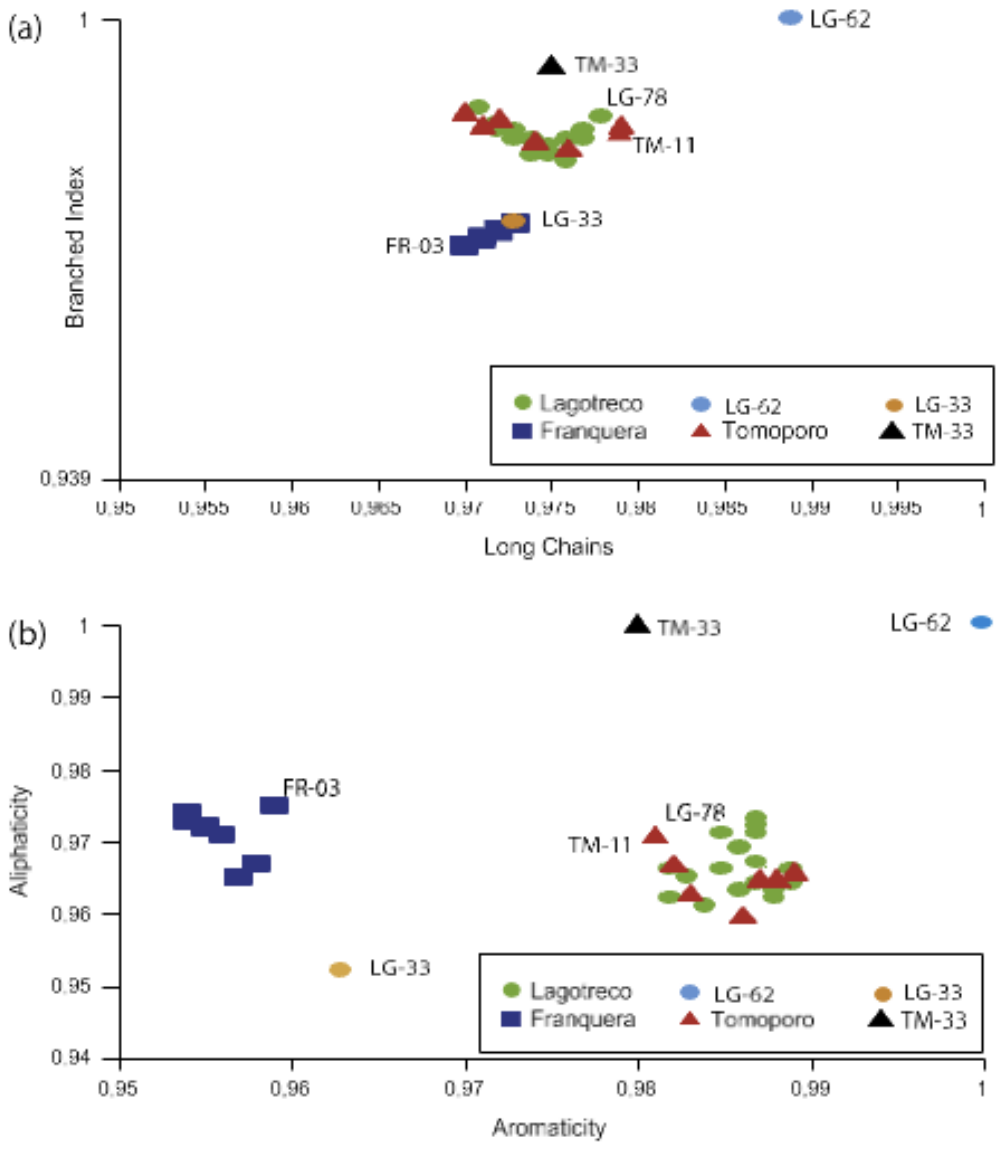

1. Conclusions

On the basis of our findings, we conclude that the mixed oils studied fall into two groups (except the three ‘‘anomalous” oils: LG-33, LG-62, and TM-33). Furthermore, we found that all the samples derived from two pulses of hydrocarbon generation and showed evidence of paleobiodegradation. All these oils also belong to the same genetic type and were originated from the same calcareous source rocks (La Luna Formation) deposited in an anoxic marine environment. In addition, we have tentatively established that VLF-3020 oil represents the contribution of the unaltered end-member oil-type. Petroleum accumulation in the Misoa B4 reservoir could be explained by vertical migration of hydrocarbons from the Cretaceous La Luna

Formation to this reservoir through the faults that delimit the Ceuta Southeast Area.
Gas chromatographic fingerprints and subsequent star diagrams clearly reveal the barrier effect of the Corredor 1 fault, which defines two separate compartments (Franquera field and Area 8 South) within the Misoa B4 reservoir rock in the Ceuta Southeast Area. Nevertheless, reservoir discontinuities in the Lagotreco and Tomoporo fields can be assessed more accurately using the FTIR method, which denotes a very good homogenization of crude oils (except the three ‘‘anomalous” oils) across the faults that cut Area 8 South in Blocks I to V and horizontal connectivity between sand bodies. Finally, the permeability baffle/barrier effect is present within the Misoa B4 reservoir rock in Blocks I and III, with no connectivity between the LG-33, LG-62, and TM-33 wells and the other wells in Area 8 South. These latter four oil groups are consistent with the results from several molecular parameters and bulk geo- chemical properties.

Acknowledgments

This study was partially found by the Development Council of the University of Zulia (CONDES-LUZ), through the Research Pro- ject No. CC-0555-13. Authors thank J. Amaroy (PDVSA) and A. Lara-Gonzalo for access to the samples and for her assistance, respectively. We are also grateful to the anonymous reviewers for their comments which helped us to improve the original manuscript.

Appendix A. Main terpanes, steranes, diasteranes and triaromatic steroids identified in the fragmentograms

1	C_{20}-Tricyclic terpane	39	17a(H),21b(H)-29-Pentahomohopane 22S
2	C_{21}-Tricyclic terpane	40	17a(H),21b(H)-29-Pentahomohopane 22R
3	C_{22}-Tricyclic terpane	41	13b(H),17a(H)-Diacholestane 20S
4	C_{23}-Tricyclic terpane	42	13b(H),17a(H)-Diacholestane 20R
5	C_{24}-Tricyclic terpane	43	5a(H),14a(H),17a(H)-Cholestane 20S[a]
6	C_{25}-Tricyclic terpane 17R + 17S	44	5a(H),14b(H),17b(H)-Cholestane 20R[a]
7	C_{24}-Tetracyclic terpane	45	5a(H),14 b(H),17b(H)-Cholestane 20S
8	C_{26}-Tricyclic terpane 17R	46	5a(H),14a(H),17a(H)-Cholestane 20R
9	C_{26}-Tricyclic terpane 17S	47	13b(H),17a(H)-Diastigmastane 20R
10	C_{28}-Tricyclic terpane 17R	48	13a(H),17bH)-Diastigmastane 20S
11	C_{28}-Tricyclic terpane 17S	49	5a(H),14a(H),17a(H)-Ergostane 20S
12	C_{29}-Tricyclic terpane 17R	50	5a(H),14b(H),17b(H)-Ergostane 20R[a]
13	C_{29}-Tricyclic terpane 17S	51	5a(H),14b(H),17b(H)-Ergostane 20S
14	18a(H)-22,29,30-Trisnorneohopane	52	5a(H),14a(H),17a(H)-Ergostane 20R
15	17a(H),21b(H)-25,28,30-Trisnorhopane	53	5a(H),14a(H),17a(H)-Stigmastane 20S
16	17a(H)-22,29,30-Trisnorhopane	54	5a(H),14b(H),17b(H)-Stigmastane 20R
17	17a(H),21b(H)-25,30-Bisnorhopane	55	5a(H),14b(H),17b(H)-Stigmastane 20S
18	C_{30}-Tricyclic terpane 17R	56	5a(H),14a(H),17a(H)-Stigmastane 20R

19	C_{30}-Tricyclic terpane 17S	57	Dibenzothiophene
20	17a(H),21b(H)-28,30-Bisnorhopane	58	4-Methyldibenzothiophene
21	17a,21b(H)-25-Norhopane	59	3-Methyldibenzothiophene[a]
22	17b(H),21a(H)-28,30-Bisnorhopane	60	1-Methyldibenzothiophene
23	C(14a)-Homo-26-nor-17a(H)-hopane?	61	20-Triaromatic steroid hydrocarbon
24	17a(H),21b(H)-30-Norhopane	62	21-Triaromatic steroid hydrocarbon
25	18a(H)-30-Norneohopane	63	26-Triaromatic steroid hydrocarbon 20S
26	17b(H),21a(H)-30-Normoretane	64	26 (20R) + 27 (20S)-triaromatic steroid
27	17a(H),21b(H)-Hopane	65	28-Triaromatic steroid hydrocarbon 20S
28	17b(H),21a(H)-Moretane	66	27-Triaromatic steroid hydrocarbon 20R
29	17a(H),21b(H)-29-Homohopane 22S	67	28-Triaromatic steroid hydrocarbon 20R
30	17a(H),21b(H)-29-Homohopane 22R	68	Phenanthrene
31	17b(H),21a(H)-29-Homomoretane 22S+22R	69	3-Methylphenanthrene
32	Gammacerane?	70	2-Methylphenanthrene
33	17a(H),21b(H)-29-Bishomohopane 22S	71	9-Methylphenanthrene
34	17a(H),21b(H)-29-Bishomohopane 22R	72	1-Methylphenanthrene
35	17a(H),21b(H)-29-Trishomohopane 22S	73	2-Methylnaphthalene
36	17a(H),21b(H)-29-Trishomohopane 22R	74	1-Methylnaphthalene
37	17a(H),21b(H)-29-Tetrahomohopane 22S	75	2-Ethylnaphthalene
38	17a(H),21b(H)-29-Tetrahomohopane 22R	76	1-Ethylnaphthalene

[a] Peak co-elution.

References

[1] Alberdi M, López L. Biomarker 18a(H)-oleanane: a geochemical tool to assess Venezuelan petroleum systems. J S Am Earth Sci 2000;13:751–60.

[2] Alcalá M. Evaluación de la unidad petrolífera B-1 de la formación Misoa entre las áreas de Franquera y La Ceiba occidente. BSc Thesis. Venezuela: Universidad de Zulia; 2013. p. 94.

[3] ASTM. Standard test method for sediment in fuel oils by the centrifugation method: annual book of the American society for testing materials standards, vol. 05.01 and 05.02. West Conshohocken, Pennsylvania: ASTM International; 2004.

[4] ASTM. Standard test method for API gravity of crude petroleum and petroleum products (hydrometer method). West Conshohocken: ASTM International; 2006.

[5] ASTM. Standard test method for n-heptane insolubles: annual book of the American society for testing materials standards, vol. 05.01 and 05.02. West Conshohocken, Pennsylvania: ASTM International; 2007.

[6] ASTM. Standard test method for sulfur in petroleum and petroleum products by energy dispersive X-ray fluorescence spectrometry. West Conshohocken: ASTM International; 2010.

[7] Benkovics L, León F, Sarzalejo S, Luna F, Peña A, Díaz J, et al. Geologic structure and deformation sequence of the Barúa-Motatan area, eastern margin of Maracaibo basin, Zulia Oriental, northern Venezuelan Andes. Sociedad Venezolana de Geólogos, Caracas, Mem. VII Simposio Bolivariano. Exploración Petrolera de las Cuencas Subandinas; 2000. p. 150–60.

[8] Bennett B, Larter S. Biodegradation scales: applications and limitations. Org Geochem 2008;39:1222–8. Beroiz C, Permanyer A. Hydrocarbon habitat of the Sedano trough, Basque- Cantabrian Basin, Spain. J Pet Geol 2011;34:387–410.

[9] Boesi T, Galea F, Rojas G, Lorente MA, Duran I, Velásquez M. Stratigraphic study of the North Andean Flank. In: III Bolivarian symposium: petroleum exploration of the sub-andean basin. Caracas; March 13–16, 1988. p. 1–41.

[10] Bracho E. Geoquímica de crudos cretácicos del lago de Maracaibo. MSc Thesis. Maracaibo: Universidad del Zulia; 2010. p. 187.

[11] Boreham CJ, Crick IH, Powell TG. Alternative calibration of the methylphenanthrene index against vitrinite reflectance: application to maturity measurements on oils and sediments. Org Geochem 1988;12:289–94.

[12] Cassani F, Gallango O, Talukdar S, Vallejos C, Ehrmann U. Methylphenanthrene maturity index of marine source rock extracts and crude oils from the Maracaibo Basin. Org Geochem 1988;13:73–80.

[13] Castillo MV. Structural analysis of Cenozoic fault systems using 3D seismic data in the southern Maracaibo Basin, Venezuela. PhD dissertation. Austin: The University of Texas; 2001. p. 189.

[14] Castillo M, Mann P. Cretaceous to Holocene structural stratygraphic development in south Lake Maracaibo, Venezuela, inferred from well and three-dimensional seismic data. AAPG Bull 2006;90:529–65.

[15] De la Cruz C, Márquez N, Escobar M, Segovia S. An improved chromatographic method for the separation of saturated hydrocarbons, aromatic hydrocarbons, resins and asphaltenes from heavy crude oils. In: 213th American Chemical Society National Meeting. San Francisco; April 13–17, 1997. p. 416–8.
[16] De Toni B, Loureiro D, Colletta B, Roure F. Structural synthesis and tectonic evolution of the Maracaibo and Barinas-Apure basins, Western Venezuela. Paper 90951 presented at the AAPG International Conference and Exhibition, Caracas; September 8–11, 1996. Dzou LI, Noble RA, Sentfle JT. Maturation effects on absolute biomarker concentration in a suite of coals and associated vitrinite concentrates. Org Geochem 1995;23:681–97.
[17] Erlich RN, Macsotay O, Nederbragt AJ, Lorente MA. Palaeoecology, palaeogeography and depositional environments of upper cretaceous rocks of western Venezuela. Palaeogeogr Palaeoclimatol Palaeoecol 1999;153:203–38.
[18] Escalona A, Mann P. An overview of the petroleum system of Maracaibo Basin. AAPG Bull 2006;90:653–74.
[19] Escobar M, Márquez G, Inciarte S, Rojas J, Esteves I, Malandrino G. The organic geochemistry of oil seeps from the Sierra de Perijá eastern foothills, Lake Maracaibo Basin, Venezuela. Org Geochem 2011;42:727–38.
[20] Everitt BS. Cluster analysis. In: Arnold Edward, editor. Multivariate statistics. London: Oxford University Press; 1993. p. 42–50.
[21] Fernández E, Marcano O. Diseño de pruebas de inyección de agua en las arenas B4 del yacimiento Eoceno B-Superior, Campo Ceuta. BSc Thesis. Maracaibo: Universidad del Zulia; 2003. p. 91.
[22] Galarraga F, Urbani F, Escobar M, Márquez G, Martínez M, Tocco R. Main factors controlling the compositional variability of seepage oils from Trujillo State, Western Venezuela. J Pet Geol 2010;33:255–68.
[23] Grobas J. Caracterización geoquímica y evolución del sistema petrolífero en el sureste de la Cuenca del Lago de Maracaibo. Tesis de Grado. Caracas: Universidad Central de Venezuela; 2008. p. 82.
[24] Guliano M, Mille G, Kister J, Muller JF. Étude des spectres IRTF de charbons français déminéralisés et de leurs macéraux. J Chim Phys 1988;85:963–70.
[25] Hakimi MH, Abdullaha WH, Shalabya MR. Organic geochemical characteristics of crude oils from the Masila Basin, eastern Yemen. Org Geochem 2011;42:465–76.
[26] Huang HP, Bowler BFJ, Oldenburg TBP, Larter SR. The effect of biodegradation on polycyclic aromatic hydrocarbons in reservoired oils from the Liaohe basin, NE China. Org Geochem 2004;35:1619–34.
[27] Hughes WB. Use of thiophenic organosulphur compounds in characterizing of oils derived from carbonate versus siliciclastic sources. In: Palacas G, editor. Petroleum geochemistry and source rock potential of carbonate rocks. AAPG Studies in Geology, vol. 18; 1984. p. 181–96.
[28] Hughes WB, Holba AG, Dzou LIP. The ratios of dibenzothiophene to phenanthrene and pristane to phytane as indicators of depositional environment and lithology of petroleum source rocks. Geochim Cosmochim Acta

1995;59:3581–98.
[29] Hunt JM. Petroleum geochemistry and geology. 2nd ed. San Francisco: Freeman and Company; 1996. p. 617.
[30] Jewell DM, Albaugh EW, Davis BE, Ruberto RG. Integration of chromatographic and spectroscopic techniques for the characterization of residual oils. Ind Eng Chem Fundam 1974;13:278–82.
[31] Kaufman RL, Ahmed AS, Elsinger RL. Gas chromatography as a development and production tool for fingerprinting oils from individual reservoirs: applications in the Gulf of Mexico. In: Gulf coast section of the society of economic paleontologists and mineralogists foundation 9th annual research conf. proc.; 1990. p. 263–82.
[32] Lazarde N. Estudio de Factibilidad para la Inyección de Agua en el Yacimiento Eoceno B-Superior VLG-3729 en el Campo Ceuta, Area 8 Sur, utilizando Simulación Numérico. Tesis Grado, Caracas: Universidad Central de Venezuela; 2000. p. 101.
[33] Lewan MD. Factors controlling the proportionality of vanadium to nickel in crude oils. Geochim Cosmochim Acta 1984;48:2231–8.
[34] Lewan MD, Maynard JB. Factors controlling enrichment of vanadium and nickel in the bitumen of organic sedimentary rocks. Geochim Cosmochim Acta 1982;46:2547–60.
[35] Linares R. Integración del yacimiento C-2/VLE-326/455 dentro del modelo geológico del bloque V Lamar, Cuenca del Lago de Maracaibo, Estado Zulia. Trabajo especial de Grado. Caracas: Universidad Central de Venezuela; 2003. p. 112.
[36] Lorenzo E. Geoquímica orgánica del petróleo en la región sureste de la Cuenca del Lago de Maracaibo (Venezuela). PhD Thesis. Huelva (España): Universidad de Huelva; 2014. p. 247.
[37] Lugo J, Mann P. Jurassic-eocene tectonic evolution of Maracaibo basin, Venezuela, vol. 62. AAPG memoir; 1995. p. 699–725.
[38] Macellari CE. Cretaceous paleogeography and depositional cycles of western South America. J S Am Earth Sci 1988;1:373–418.
[39] Mackenzie AS, Maxwell JR. Assessment of thermal maturation in sedimentary rocks by molecular measurements. In: Brooks J, editor. Organic maturation studies and fossil fuel exploration. London: Academic Press; 1981. p. 239–54.
[40] Mackenzie AS, Rullkoetter J, Welte DH, Mankiewicz P. Reconstruction of oil formation and accumulation in North Slope, Alaska, using quantitative gas chromatography–mass spectrometry. In: Claypool GE, editor. Alaska north slope oil-rock correlation study; analysis of north slope crude. American Association of Petroleum Geologists; 1985. p. 319–77.
[41] Mann P. Caribbean sedimentary basins: classification and tectonic setting from jurassic to present. Caribbean basins. Sedimentary basins of the world, vol. 4. Elsevier; 1999. p. 3–31.
[42] Mann P, Escalona A, Castillo M. Regional geologic and tectonic setting of the Maracaibo supergiant basin, Western, Venezuela. AAPG Bull 2006;90:445–77.
[43] Mason PC, Burwood R, Mycke B. The reservoir geochemistry and petroleum

charging histories of Palaeogene-reservoired fields in the Outer Witch Ground Graben. In: Cubitt JM, England WA, editors. The geochemistry of reservoirs. London: Geological Society of London; 1995. p. 281–301. Murillo WA. Caracterización geoquímica de crudos y rocas de las formaciones La Luna, Misoa y Colón en la zona oriental del Estado Zulia. Tesis de Grado. Caracas: Universidad Central de Venezuela; 2008. p. 126.

[44] Olivares C, Molina A, Vargas C, Espinoza S, Hung F. Regional model of petroleum charge, timing and preservation in the southeast portion of the Maracaibo Basin, Venezuela. In: Abstracts of 25th international meeting on organic geochemistry, Interlaken; 2009. p. 436.

[45] Palacios C. Caracterización petrográfica de carbonatos del campo de Mara. Cuenca de Maracaibo, Estado Zulia. Trabajo final de Grado. Universidad de Zulia; 2006. p. 181.

[46] Palmer SE. Effect of water washing on $C15^{+}$ hydrocarbons fraction of crude oils from northwest Palawan, Phillipines. AAPG Bull 1984;68:137–49.

[47] Parnaud F, Gou Y, Pascual JC, Capello MA, Truskowski I, Passalaqua H. Stratigraphic synthesis of Western Venezuela. In: Tankard AJ, Suárez Soruco R, Welsink HJ, editors. Petroleum basins of South America. vol. 62. AAPG Memoir; 1995. p. 681–98.

[48] Permanyer A, Douifi L, Dupuy N, Lahcini A, Kister J. FTIR and SUVF spectroscopy as an alternative method in reservoir studies. Application to Western Mediterranean oils. Fuel 2005;84:159–68.

[49] Permanyer A, Douifi L, Lahcini A, Lamontagne J, Kister J. FTIR and SUVF spectroscopy applied to reservoir compartmentalization: a comparative study with gas chromatography fingerprints results. Fuel 2002;81:861–6.

[50] Permanyer A, Rebufa C, Kister J. Reservoir compartmentalization assessment by using FTIR spectroscopy. J Petrol Sci Eng 2007;58:464–71.

[51] Permanyer A, Salas R. Integrated thermal model, diagenetic history and oil correlation in the Western Mediterranean, Spain. In: Abstracts of IV ALAGO workshop – basin modeling. Buenos Aires; October 16–19, 2005. p. 1–5.

[52] Peters K, Walters CC, Moldowan JM. The biomarker guide: biomarkers and isotopes in petroleum systems and earth history. 2nd ed. Cambridge University Press; 2005. p. 1132.

[53] Philp RP, Mansuy L. Petroleum geochemistry: concepts, applications, and results. Energy Fuels 1997;11:749–60.

[54] Radke M. Application of aromatic compounds as maturity indicators in source rocks and crude oils. Mar Pet Geol 1988;5:224–36.

[55] Radke M, Welte DH. The methylphenantrene index (MPI): a maturity parameter based on aromatic hydrocarbons. In: Bjoroy M, Albrecht C, Cornford C, de Groot K, Eglinton G, Galimov E, Leythaeuser D, Pelet R, Rullkoetter J, Speers G, editors. Advances in organic geochemistry. New York: J. Wiley and sons; 1983. p. 504–12.

[56] Radke M, Leythaeuser D, Teichmüller M. Relationship between rank and composition of aromatic hydrocarbons from coals of different origins. Org

Geochem 1984;6:423–30.
[57] Radke M, Welte DH, Willsch H. Geochemical study on a well in the Western Canada Basin: relation of the aromatic distribution pattern to maturity of organic matter. Geochim Cosmochim Acta 1982;46:1–10.
[58] Rodríguez I, Navarro A, Ghosh S. Nueva Frontera Exploratoria en la Cuenca Petrolífera del Lago de Maracaibo: Zulia Oriental, Venezuela Occidental. Asociación Colombiana de Geólogos y Geofísicos del Petróleo. Memorias VI Simposio Bolivariano de Exploración de Cuencas Subandinas, Cartagena; 1997. p. 565–81.
[59] Romesburg HC. Cluster analysis for researches. Belmont, US: Lifetime Learning Publications; 1984.
[60] Roure F, Colleta B, De Toni B, Loureiro D, Passalqua H, Gou Y. Within plate deformations in the Maracaibo and East Zulia basins, Eastern Venezuela. Mar Petrol Geol 1996;2:139–63.
[61] Rowland SJ, Alexander R, Kagi RI, Jones DM, Douglas DG. Microbial degradation of aromatic components of crude oils: a comparison of laboratory and field observations. Org Geochem 1986;9:153–61.
[62] Rullkötter J, Spiro B, Nissenbaum A. Biological marker characteristics of oils and asphalts from carbonate source rocks in a rapidly subsiding graben, Dead Sea, Israel. Geochim Cosmochim Acta 1985;49:1357–70.
[63] Seifert WK, Moldowan JM. Application of steranes, terpanes and monoaromatic to the maturation, migration and source of crude oils. Geochim Cosmochim Acta 1978;42:77–95.
[64] Seifert WK, Moldowan JM. Palaeoreconstruction by biological markers. Geochim Cosmochim Acta 1981;45:783–94.
[65] Sofer Z. Stable Carbon Isotope composition of crude oils: application to source depositional environments and petroleum alteration. AAPG Bull 1984;68:31–49.
[66] Sweeney J, Talukdar S, Burnham A, Vallejos C. Pyrolysis kinetics applied to prediction of oil generation in the Maracaibo Basin, Venezuela. Org Geochem 1990;16:189–96.
[67] Talukdar S, Gallango O, Ruggiero A. Venezuelan La Luna and Querecual Formations as petroleum source rocks. VI Venezuelan Geological Congress, Caracas; 1985. p. 3606–42.
[68] Talukdar S, Gallango O, Chin-A-Lien M. Generation and migration of hydrocarbons in the Maracaibo Basin, Venezuela: an integrated basin study. Org Geochem 1986;10:261–79.
[69] Talukdar S, Marcano F. Petroleum system of the Maracaibo Basin, Venezuela. In: Magoon LB, Dow WG, editors. The petroleum system – for source to trap, vol. 60. Tulsa: American Association of Petroleum Geologists Memoir; 1994. p. 463–81.
[70] Thompson KFM. Fractionated aromatic petroleums and the generation of gas-condensates. Org Geochem 1987;11:573–90.
[71] Tissot BP, Welte DH. Petroleum formation and occurrence. 2nd ed. New Tocco

R, Parnaud F, Gallango O, Alberdi M, Passalacqua H. Geochemical modelling of the principal source rocks of the Barinas and Maracaibo Basins, Western Venezuela. Bull Venezuelan Soc Geol 1997;22:17–28.

[72] Urbina ER. Determinación de registros psudo-sónicos a partir de registros de resistividad en los campos Barúa, Motatán y Tomopoto. Trabajo Especial de Grado. Universidad Central de Venezuela; 2001. p. 153.

[73] van Graas GW. Biomarker maturity parameters for high maturities: calibration of the working range up to the oil/condensate threshold. Org Geochem 1990;16:1025–32.

[74] Volkman JK, Alexander R, Kagi RI, Rowland SJ, Sheppard PN. Biodegradation of aromatic hydrocarbons in crude oils from the Barrow Sub-basin of Western Australia. Org Geochem 1984;6:619–32.

[75] Walton WM. Contributions of the AVGMP Maracaibo basin eocene nomenclature comittee: the informal units of the subsurface eocene. Venez Geol, Min Petrol, Bol Inform 1967;10:21–30.

[76] Wenger LM, Davis CL, Isaksen GH. Multiple controls on petroleum biodegradation and impact on oil quality. SPE Reservoir Eval Eng 2002;5:375–83.

[77] Young GA. Correlation of the oligo-miocene formations in the districts of urdaneta and Perijá, State of Zulia. Assoc Venez Geol, Min Petrol Bol Inform 1958;1:116–35.

[78] Zapata I. Interpretación sísmica structural 3D y uso de atributos sísmicos en el Cretácico, bloques IX y XIV del Lago de Maracaibo. Tesis de Grado. Maracaibo: Universidad del Zulia; 2001. p. 129.